



**HAL**  
open science

# Ascending vestibular pathways to parietal areas MIP and LIPv and efference copy inputs from the medial reticular formation: Functional frameworks for body representations updating and online movement guidance

Gabriella Ugolini, Vincent Prevosto, Werner Graf

## ► To cite this version:

Gabriella Ugolini, Vincent Prevosto, Werner Graf. Ascending vestibular pathways to parietal areas MIP and LIPv and efference copy inputs from the medial reticular formation: Functional frameworks for body representations updating and online movement guidance. *European Journal of Neuroscience*, 2019, 50 (6), pp.2988-3013. 10.1111/ejn.14426 . hal-03070565

**HAL Id: hal-03070565**

**<https://hal.science/hal-03070565v1>**

Submitted on 15 Dec 2020

**HAL** is a multi-disciplinary open access archive for the deposit and dissemination of scientific research documents, whether they are published or not. The documents may come from teaching and research institutions in France or abroad, or from public or private research centers.

L'archive ouverte pluridisciplinaire **HAL**, est destinée au dépôt et à la diffusion de documents scientifiques de niveau recherche, publiés ou non, émanant des établissements d'enseignement et de recherche français ou étrangers, des laboratoires publics ou privés.



Distributed under a Creative Commons Attribution 4.0 International License

Article type : Research Report

**Journal section: Developmental neuroscience and Neurosystems**

**Section Editor: Dr Ying-Shing Chan**

Ascending vestibular pathways to parietal areas MIP and LIPv and efference copy inputs from the medial reticular formation: functional frameworks for body representations updating and online movement guidance.

Gabriella Ugolini<sup>1</sup>, Vincent Prevosto<sup>1,2,3</sup>, Werner Graf<sup>4</sup>.

<sup>1</sup> Paris-Saclay Institute of Neuroscience (UMR9197) CNRS - Université Paris-Sud, Université Paris-Saclay, 91198 Gif-sur-Yvette, FR;

<sup>2</sup> Department of Biomedical Engineering, Pratt School of Engineering, and <sup>3</sup> Department of Neurobiology, Duke School of Medicine, Duke University, Durham, NC, USA;

<sup>4</sup> Department of Physiology and Biophysics, Howard University, Washington DC, USA.

**Corresponding author:** Dr Gabriella Ugolini, Paris-Saclay Institute of Neuroscience (UMR9197), Bât 32 CNRS, 1 av de la Terrasse, 91198 Gif sur Yvette, France.

Tel : + 33 1 6982 4158. e-mail: [gabriella.ugolini@inaf.cnrs-gif.fr](mailto:gabriella.ugolini@inaf.cnrs-gif.fr)

This article has been accepted for publication and undergone full peer review but has not been through the copyediting, typesetting, pagination and proofreading process, which may lead to differences between this version and the Version of Record. Please cite this article as doi: 10.1111/ejn.14426

This article is protected by copyright. All rights reserved.

**Running title:** Vestibular and reticular inputs to MIP and LIPv

**Keywords:** monkey, VIP, Scarpa, virus, systems neuroscience

## **ABSTRACT**

The posterior parietal cortex (PPC) serves as a sensorimotor interface by integrating multisensory signals with motor related information for generating and updating body representations and movement plans. Using retrograde transneuronal transfer of rabies virus combined with a conventional tracer, we identified direct and polysynaptic pathways to two PPC areas, the rostral medial intraparietal area (MIP) and the ventral part of the lateral intraparietal area (LIPv) in macaque monkeys. We found that rostral MIP and LIPv receive ascending vestibular pathways, and putative efference copy inputs disynaptically from the medullary medial reticular formation (MRF) where reticulospinal pathways to neck and arm motoneurons originate. LIPv receives minor disynaptic vestibular inputs, and substantial projections from the head movement-related rostral MRF, consistent with head gain modulation of LIPv activity and a role in planning gaze shifts. Rostral MIP is the target of prominent disynaptic pathways from reaching- and head movement-related MRF domains, and major ascending vestibular pathways trisynaptically from both labyrinths, explaining prominent vestibular responses and discrimination between active and passive movements demonstrated in rostral MIP and in the neighboring ventral intraparietal area, which are heavily interconnected. The findings that rostral MIP (belonging to the ‘parietal reach region’), receives vestibular inputs as directly as classical vestibular areas, via a parallel channel, and efference copy signals pathways from MRF reticulospinal domains that belong to reach and head movement networks have important implications for the understanding of

the role of the PPC in updating body representations and internal models for online guidance of movement.

## INTRODUCTION

The posterior parietal cortex (PPC), which is part of the visual dorsal stream and has reciprocal connections with frontal lobe motor areas, is a major sensorimotor interface, which maintains dynamic representations of internal and extrapersonal space and participates in planning and execution of sensory-guided goal-directed movements (Andersen, 1997; Rushworth *et al.*, 1997; Grefkes *et al.*, 2004; Buneo & Andersen, 2006; Filimon *et al.*, 2009). Integration of internal information (proprioceptive, vestibular, motor) and external signals (visual, tactile, auditory) is crucial for these functions. Damage to the PPC can cause a variety of disorders that result from defective multisensory integration; depending on the location of the lesion, they affect bodily self-consciousness and/or spatial awareness, as in neglect (Vallar, 1998; Danckert & Ferber, 2006; Lopez *et al.*, 2008), or compromise sensorimotor guidance of movement as in optic ataxia (Andersen *et al.*, 2014). Clarifying the type and origin of inputs to the PPC is critical for understanding the sensorimotor mechanisms supporting its command operations.

Cortical integration of vestibular signals evoked by self-motion is important for a variety of self-related perceptual and cognitive functions (Andersen, 1997; Lopez *et al.*, 2008; Blanke *et al.*, 2015). Vestibular signals are transmitted to multiple cortical areas by vestibulothalamic pathways and cortico-cortical connections (Lopez & Blanke, 2011). In the PPC, human neuroimaging studies showed intraparietal sulcus (IPS) activation after vestibular stimulation (reviewed by Lopez & Blanke, 2011). Evidence has also been provided that the human IPS uses vestibular signals for fast online adjustment of goal-directed arm movements (Reichenbach *et al.*, 2016). In monkeys, vestibular responses in the IPS have

been recorded in the ventral intraparietal area (VIP) and in the rostral medial intraparietal area (MIP) (Bremmer *et al.*, 2001, 2002; Schlack *et al.*, 2002; Klam & Graf, 2003, 2006; Chen *et al.*, 2011).

We have studied the origin of direct and polysynaptic inputs to rostral MIP and to the ventral part of the lateral intraparietal area (LIPv) in macaque monkeys, using retrograde transneuronal transfer of rabies virus combined with a conventional tracer (Fig. 1) (Ugolini 1995, 2010, 2011; Prevosto *et al.*, 2009, 2010, 2011). The targeted rostral MIP, at midpoint level of the medial bank of the IPS, is part of the functionally defined ‘parietal reach region’, (Andersen *et al.*, 2014). It corresponds to the rostral part of the myeloarchitectonically defined MIP (Colby *et al.*, 1988; Bakola *et al.*, 2017), which according to other nomenclature, is regarded as part of 5v (e.g., Hwang *et al.*, 2012, 2014), caudal PEip, or the middle third of PEa (see Prevosto *et al.*, 2010; Bakola *et al.*, 2017). LIPv is part of the ‘parietal eye field’ (Buneo & Andersen, 2006; Bisley & Goldberg, 2010); it differs from dorsal LIP with regard to myelo- and cytoarchitecture, visual field representation, connectivity and functional role (Lynch *et al.*, 1985; Blatt *et al.*, 1990; Lewis & Van Essen, 2000a,b; Ben Hamed *et al.*, 2001; Liu *et al.*, 2010; Chen *et al.*, 2016).

Here, we demonstrate that rostral MIP receives major ascending vestibular inputs through a trisynaptic pathway from both labyrinths (i.e., from Scarpa’s ganglia to second order vestibular neurons issuing vestibulothalamic pathways, and then thalamocortical neurons). Conversely, LIPv receives minor ascending vestibular inputs. These findings have important implications for the understanding of vestibular information processing on reference frame transformations for action in the PPC and online control of goal-directed arm movements. Because vestibular units in the ventral posterior thalamus can distinguish between active and passive movements (Dale & Cullen, 2017), ascending vestibular pathways to rostral MIP explain the distinction between active and passive movements

demonstrated in rostral MIP and VIP (Klam & Graf, 2006), providing a correlate for ensuring perceptual stability and effective motor actions.

Remarkably, our study also revealed that rostral MIP and LIPv receive disynaptic pathways from the medullary medial reticular formation (MRF), which target most prominently rostral MIP, but also provide substantial and topographically distinct inputs to LIPv. These pathways are suited to carry efference copy signals related to arm and head movements, because they originate from reticulospinal MRF regions that belong to reaching and head movement networks. MRF efference copy pathways to the PPC have the required characteristics to contribute to internal models for online motor control operations in the PPC, together with ascending vestibular pathways and cerebellar output channels (Prevosto *et al.*, 2010). Preliminary accounts of some of these findings have been reported earlier (Prevosto *et al.*, 2006).

## **MATERIAL AND METHODS**

Experiments were conducted in 3 adult macaque monkeys (1 *Macaca fascicularis*, 2 *Macaca mulatta*). The animals were purpose-bred and purchased from authorized suppliers. The experiments were carried out at the appropriate biosafety containment level. Animal care and experimental procedures were approved by the relevant institutional Bioethical Committees (Regional Committee of Biomedical Ethics, Centre National de la Recherche Scientifique, and French Ministry of Agriculture Veterinary Services) and conformed with national laws and the Council Directive 2010/63EU of the European Parliament and the Council of 22 September 2010 on the protection of animals used for scientific purposes, as well as the European Communities Council Directive of 24 November 1986 (86/609/EEC) concerning biosafety and use of laboratory animals in research, and "Principles of Laboratory Animal Care" (NIH publication No. 86-23, revised 1985). Details on preparation of rabies virus, handling of

animals, and the methodology for transneuronal tracing using rabies virus were described previously (Ugolini, 1995, 2010, 2011; Ugolini *et al.*, 2006; Prevosto *et al.*, 2009, 2010, 2011).

### **Surgical procedures, injections and postoperative care**

Surgery was performed aseptically under general anesthesia. After premedication with Valium (10 mg) and Atropine (0.5 mg), anesthesia was induced with Ketamine (30 mg/kg i.m.) and Acepromazine (0.5 mg/kg i.m.); after establishing venous access, the anesthetic Propofol was administered intravenously during the entire procedure (induction dose, 10 mg/kg, maintenance dose 15 mg/kg/h). The monkey's head was fixed in a stereotaxic headholder. Access to the intraparietal sulcus (IPS) areas (VIP, rostral MIP and LIPv) of the left hemisphere (Fig. 1) was gained via a previously implanted recording chamber, which was equipped with a Teflon grid for electrode placement, thereby allowing highly reproducible electrode penetrations. Injections were made at the end of long-term electrophysiological recordings (Klam & Graf, 2006), and targeted at stereotaxic coordinates of previously recorded responses. As described earlier (Prevosto *et al.*, 2009, 2010, 2011), neurons at the rostral MIP injection site were characterized by prominent vestibular responses, sensitivity to somatosensory stimulation on the arms and hands (Klam & Graf, 2003, 2006) and bimodal somatosensory/visual responses (e.g., Colby & Duhamel 1991; Iriki *et al.*, 1996; Graziano *et al.*, 2000). Neurons at the LIPv injection site showed characteristic visual and eye movement related activities (Blatt *et al.*, 1990, Ben Hamed *et al.*, 2001), weak vestibular responses (Andersen, 1997), and no somatosensory responses characteristic of VIP (Colby & Duhamel, 1991).

A mixture of rabies virus (CVS strain,  $5.96 \times 10^{10}$  PFU/ml) and the conventional tracer Cholera toxin B fragment (CTB low salt, end concentration 0,03%) (List Biological Labs, Campbell, CA) was injected in a single dose (2  $\mu$ l delivered over 30 minutes) into rostral MIP (2 monkeys) or LIPv (1 monkey) at midpoint of the rostrocaudal length of the IPS (Fig. 1) using a Hamilton syringe driven by a micromanipulator. The injection needle was left in place for more than 30 minutes after the end of the injection. After recovery from general anesthesia, the animals behaved normally without any clinical or behavioral signs of infection for the entire duration of the study (Prevosto *et al.*, 2009, 2010, 2011).

### **Time points of transfer**

Animals were euthanized for histological examination 2.5 days (experiments MIP-2 and LIPv-1) and 3 days (MIP-1) after intracortical injection of the rabies virus/CTB mixture. As shown earlier (Prevosto *et al.*, 2009, 2010, 2011), these times points are sufficient for labeling of first-order neurons (CTB) and simultaneous retrograde transneuronal labeling of second-order neurons (2.5 days), and third-order neurons (3 days) with rabies virus (see Ugolini, 2010) (Figs 1 and 2). At the designated time points, the animals were given a lethal dose of pentobarbital (30 mg/kg i.v.) after induction of deep general anesthesia as described above. They were perfused transcardially with 2 liters of phosphate buffered saline (PBS) (pH 7.4), followed by 3.5 liters of 4% paraformaldehyde in 0.1 M phosphate buffer (PB) (pH 7.4) and 4 liters of 10% sucrose in 0.1 M PB (pH 7.4).

### **Tissue processing and immunohistochemistry**

Brains were removed from the cranium, including the left and right vestibular (Scarpa's) ganglia, and cut stereotaxically in two blocks (13 mm anterior of the interaural line) in the frontal plane. Tissue blocks (the caudal one also including Scarpa's ganglia) were



cryoprotected and gelatin-embedded as described previously (Ugolini *et al.*, 2006), and cut in frozen serial sections (50  $\mu\text{m}$ ), which were collected free-floating in 8 parallel series. In two series (200  $\mu\text{m}$  spacing), rabies virus was visualized immunohistochemically using a monoclonal antibody directed against the rabies P protein (diluted 1:1000, overnight incubation at 4° C) and the peroxidase anti-peroxidase method as described previously (Ugolini *et al.*, 2006). After reactions, sections were mounted on gelatin-coated slides, air dried, counterstained with 0.1-0.5% Cresylviolet (Sigma-Aldrich, France) and coverslipped with Entellan (Merck, Whitehouse Station, NJ). In an adjoining series of sections, CTB labeling was visualized using as primary antibody goat anti-cholera toxin B subunit (List Biological Labs, Campbell, CA) (diluted 1:5000, 8 days incubation at 4° C) and the peroxidase anti-peroxidase method as described previously (Prevosto *et al.*, 2010). Sections were mounted on gelatin-coated slides, air dried and coverslipped with Entellan (Merck, Whitehouse Station, NJ). Another series of sections was stained for myelin with gold chloride (Prevosto *et al.*, 2010).

### **Data Analysis**

Every fourth section was examined for rabies immunolabeling and every eighth sections for CTB immunolabeling. Labeled neurons were analyzed and counted using a computer-assisted plotting and three-dimensional reconstruction software (Neurolucida, MBF Bioscience, Williston, VT) on a computer linked to a light microscope. Three-dimensional reconstructions of the injection area were created using Neurolucida, by stacking in register digital plots of immunolabeled serial sections. Solid reconstructions were visualized using the associated Solid Model software and exported into Adobe Illustrator. High resolution composites of digital images were captured using a video camera (Lumenera, Ottawa, CN) coupled to the microscope and the Virtual Slice module of Neurolucida (MBF Bioscience, Williston, VT). Contrast, brightness and sharpness of digital photomicrographs were

adjusted, if necessary, using Adobe Photoshop CS5. Illustrations were prepared using Adobe Illustrator.

## RESULTS

We have demonstrated earlier in this model that injecting intracortically a mixture of the conventional tracer CTB (0,03 %) and rabies virus makes it possible to determine the precise extent of the injection site and to identify simultaneously first-order (CTB) and higher-order projections (rabies virus) to the injected cortical areas, without altering the uptake and transport of either tracer (Prevosto *et al.*, 2009, 2010; 2011; Ugolini, 2010).

The CTB results showed that the injection area involved exclusively the rostral part of MIP (n=2) or ventral LIP (LIPv) (n=1) at midpoint level of the rostrocaudal extent of the IPS (see Fig. 1). Cyto- and myeloarchitectonic criteria used for the identification of the injected cortical areas have been illustrated earlier (Prevosto *et al.*, 2009, 2010, 2011).

In keeping with reports of reciprocal interconnections of MIP and LIPv with VIP (Lewis & Van Essen, 2000b; Bakola *et al.*, 2017), the CTB results showed that direct projections to the injected rostral MIP originate from dorsal VIP (Fig. 3C and E); by comparison, projections to LIPv are derived from wider VIP portions, especially from ventral VIP, and are much heavier (Fig. 3A). Remarkably, we found that MIP receives major projections from the homotopic ventral MIP of the opposite hemisphere (Figs 3D and F, and 4B); conversely, homotopic callosal projections to LIPv are minor (n= 6 versus n= 352 and n=137 cells in the MIP experiments) (Figs 3B and 4B), whereas CTB cell counts in the ipsilateral thalamus do not substantially differ (Fig. 4A). This direct connectivity is relevant for the interpretation of rabies transneuronal labeling in the thalamus and brainstem (see

below). The minor callosal connectivity of LIPv is consistent with the findings that representation of the ipsilateral visual hemifield in LIP is limited to the central 5°, whereas the targeted LIPv contains a peripheral representation (Ben Hamed et al., 2001).

## **Thalamus**

We delineated the thalamic nuclei (Fig. 5) according to Olszewski's classification (1952). The distribution in the thalamus (Fig. 5) of first-order (CTB, dots) and higher-order neurons (rabies virus, dark labeling) obtained in these experiments has been illustrated earlier (Prevosto *et al.*, 2009, 2010, 2011). Thalamic labeling provided an internal control for the number of synapses crossed by the rabies tracer. Only disynaptic (second-order) projections were labeled at 2.5 days, because labeling of the reticular thalamic nucleus (Rt) occurred only ipsilaterally (second-order) (Figs 2 and 5); at this time point, rabies virus immunolabeling in the ipsilateral thalamus visualized also thalamo-cortical inputs to cortical areas of the same hemisphere that are directly connected to MIP and LIPv, including projections from vestibular areas 3a to MIP and 2v to LIPv (Prevosto *et al.*, 2011) and from VIP to both areas (see above, Fig. 3). Second-order labeling in the contralateral (right) thalamus largely mirrored the distribution of first-order (CTB) labeling ipsilaterally, as it reflected thalamo-cortical projections to MIP and LIPv of the opposite hemisphere, which are directly connected to the injected left MIP and LIPv via callosal connections (Prevosto *et al.*, 2009, 2010, 2011) (Figs 2, 3, 4 and 5). Notably, second-order labeling in the contralateral thalamus was much heavier in the MIP case (Fig. 5), because of the much stronger callosal connections of MIP compared with LIPv (Figs 3 and 4B, see above). The occurrence of an additional synaptic step at the 3 days time point was demonstrated by labeling of the contralateral Rt nucleus (trisynaptic) (Figs 2 and 5).

The CTB results showed a different topography of thalamo-cortical projections to MIP and LIPv (Figs 4A and 5). Thalamic input to rostral MIP was derived from the dorsal capping zone of the ventral posterior lateral nucleus, pars caudalis (VPLc) (see Prevosto *et al.*, 2011), portions of the ventral lateral nucleus, pars caudalis (VLc) and pars postrema (VLps), the intralaminar central lateral (CL) nucleus and the lateral portion of the medial dorsal (MD) nucleus, and from mainly dorsal and lateral portions of the lateralis posterior (LP) and anterior pulvinar (APul) nuclei (Fig. 5). Thalamic input to LIPv originated from the CL and lateral MD and largely from more caudal, medial, and ventral portions of LP and APul (Fig. 5); it also extended much more caudally in the pulvinar complex (Fig. 4A) (see Prevosto *et al.*, 2010).

Of interest for the present report is the first-order labeling obtained in thalamic nuclei that receive vestibulothalamic or reticulothalamic projections, which would explain the disynaptic (second-order) labeling obtained at 2.5 days in the vestibular nuclei (VN) and dorsal medullary MRF in the MIP and LIPv experiments (see below). Thus, a brief summary of these pathways is provided below.

Primate thalamic nuclei carrying vestibular signals include the VPLc and VPL, pars oralis (VPLo), parts of the ventral posterior inferior (VPI) and ventral posterior medial nuclei (VPM), large portions of the VL, the LP, CL, central medial (CM), APul and posterior group (Büttner & Henn, 1976; Liedgren *et al.*, 1976; Deecke *et al.*, 1977; Magnin & Fuchs, 1977; Büttner *et al.*, 1977; Büttner & Lang, 1979; Marlinski & McCrea 2008; Meng *et al.*, 2007, Meng & Angelaki 2010). In tracing studies, projections from the VN have been demonstrated only to the VPLc, VPLo, VPI, VLc, CL and lateral MD (Lang *et al.*, 1979; Büttner & Lang, 1979; Tracey *et al.*, 1980; Asanuma *et al.*, 1983a; Russchen *et al.*, 1987; Meng *et al.*, 2007). Reticulo-thalamic projections originating from the dorsal medullary MRF regions that issue

disynaptic pathways to MIP and LIPv heavily target the CL and lateral MD; patchy terminations were also found elsewhere in VL, VPL and LP-pulvinar complex (Graybiel, 1977; Matsuyama *et al.*, 1988; Ohtake, 1992; Nagata, 1986; Russchen *et al.*, 1987).

The CTB results showed that direct thalamocortical projections to rostral MIP and LIPv originate from several of the thalamic nuclei receiving projections from the VN, i.e., the VPLc and caudal VLc, the CL and lateral MD (dots in Fig. 5). Of these, CL and MD give rise to projections to both MIP and LIPv, whereas the VPLc and VLc target MIP (Fig. 5). Similarly, reticulo-thalamic projections from the labeled MRF can reach MIP and LIPv via the CL, lateral MD, VLc and VPLc and, to a lesser extent, the LP-Pulvinar complex (see above). Of these, the CL and lateral MD and LP-Pulvinar complex project to both MIP and LIPv, whereas VPLc and VLc target only MIP (Fig. 5).

### **Vestibular nuclei and reticular formation – disynaptic inputs to MIP (2.5 days)**

Retrograde transneuronal labeling in the brainstem at 2.5 days reflected disynaptic projections to MIP and LIPv via the thalamus. Of interest for the present report is the labeling obtained in the vestibular complex and medullary MRF. The results revealed major quantitative differences and some topographical differences in the vestibular and reticular populations that target disynaptically MIP and LIPv (Figs 2 and 6-10). Additional brainstem data obtained from these experiments (and partially included in the line drawings) were already described, regarding proprioceptive pathways to MIP and LIPv from the dorsal column nuclei (DCN) (see Prevosto *et al.*, 2011), ascending pathways from the horizontal eye position integrator (prepositus hypoglossi, PH), which carry eye position and velocity signals to MIP and LIPv, and a few ascending pathways from the spinal trigeminal nucleus (SpV) targeting LIPv (see Prevosto *et al.*, 2009).

## Vestibular nuclei

Neurons with disynaptic projections from the VN to MIP were seen bilaterally, with dominance *contralaterally* in the medial vestibular nucleus (MV) in the caudal half of the VN and *ipsilaterally* in the rostral part of the vestibular complex (Figs 6, 7 and 8). Their greatest number (n=386) was found in the medial vestibular (MV) nucleus, especially in its caudal half (Figs 6, 7 and 8); some labeled cells were also seen in portions of the descending vestibular (DV) (n=56), vestibular Y group (n= 23) and superior vestibular nuclei (SV; n=107) (Figs 6 and 8).

In the MV nucleus caudal pole, labeled neurons were absent (Fig. 6A) or almost exclusively *contralateral* (Figs 6B and 8). More rostrally, within the caudal half of the MV, many labeled neurons were present bilaterally, with a much greater number contralaterally (Figs 6C-G, 7E-I, and 8). Most of them were large multipolar cells, with long labeled dendrites often running in the plane of sections (Fig. 7E-I). They showed a similar topography on both sides; they were characteristically located mainly ventrally, in the magnocellular portion of the MV (MVmc) and in the neighboring parvocellular MV (MVpc) laterally and dorsally (Figs 6C-G and 7E-I). In the rostral half of the MV, labeled cells drastically reduced in numbers (Figs 6H-L, 7A and 8), and in the rostral third of the MV, they were more numerous *ipsilaterally*, in MVmc (Fig. 6J-L).

In the DV nucleus, only a few neurons were labeled in the caudal third of the nucleus on both sides (Fig. 6); more neurons were labeled at more rostral levels, especially contralaterally in the middle rostrocaudal third of the DV, and ipsilaterally in its rostral third (Figs 6, 7 and 8). Some neurons were also labeled bilaterally in the vestibular Y group (Figs 6E and 8) and particularly in the SV nucleus, especially dorsally (Figs 6F-L and 8). The large

vestibulospinal cells of the lateral vestibular (LV) nucleus were not labeled; the few medium size multipolar cells labeled near/within the LV boundaries were regarded as part of the SV and included in the SV cell counts (Figs 6 and 8).

### **Reticular formation**

A considerable number of labeled cells (n=308) were also present bilaterally in dorsal parts of the reticular formation between the levels of the abducens (VI) and hypoglossal (XII) nuclei (Figs 6, 7 and 8). The portion of the MRF containing reticulothalamic neurons that target MIP included the dorsal portion of the gigantocellular reticular formation (Gi), as well as the reticular region dorsal to Gi, lateral to the paramedian tracts and ventral to the XII, PH and VI nuclei (Figs 6 and 7), which comprises the dorsal paragigantocellular reticular formation (DPGi), the caudal end of nucleus reticularis pontis caudalis at the level of the VI nucleus, and the paramedian reticular nucleus at caudal medullary levels (levels shown in Figs 6A-D and 7I) (Langer *et al.*, 1986). To provide a shorthand for the description and because it is cytoarchitectonically similar throughout, we call this entire region DPGi, like Paxinos *et al.* (2000).

Throughout most medullary levels, labeled cells were numerous in the dorsal part of Gi and neighboring DPGi (Figs 6 and 7); they were distributed bilaterally, with a *contralateral* dominance (Figs 6A-J, 7 and 8). Labeled neurons in Gi/DPGi were generally large, multipolar cells, dispersed among many unlabeled ones (Fig. 7). Rostrally, at the level of the VI nucleus and of the genu of the facial nerve, labeled cells in the MRF were numerous in Gi and only a few in DPGi (Fig. 6K and L). In both MIP and LIPv experiments, labeling at these levels did not involve the distinct eye movement-related cell cluster (inhibitory burst neurons) which is located dorsally in DPGi, near the VI nucleus (Ugolini *et al.*, 2006).

Similarly, the cell groups embedded within the paramedian fiber tracts, which project to the flocculus and ventral paraflocculus (Langer *et al.*, 1985), were unlabeled.

In the rostral medulla, a few labeled cells of medium/large size were also present more laterally, in the dorsal portion of the lateral reticular formation (LRF), immediately ventral to the rostral MVmc, and lateral and caudal to the VI nucleus (Figs 6G-J, and 7A and D, asterisks). Eye movement-insensitive neurons were described in this small reticular region (Fuchs & Kimm, 1975), which receives a few direct otolith afferents (Newlands *et al.*, 2003).

### **Vestibular nuclei and reticular formation – disynaptic inputs to LIPv (2.5 days)**

#### **Vestibular complex**

Disynaptic projections to LIPv from the VN were much fewer (less than 1/10 of the number of cells in the vestibular complex that targeted MIP). They were derived almost exclusively from the MV (n=36), with only small numbers in the DV (n=7) and SV (n=4) and none in the vestibular Y group or LV nuclei (Figs 8, 9 and 10). As for MIP, labeled cells targeting LIPv were most numerous in the caudal half of the MV (except its caudal pole), they were located only in MVmc and neighboring lateral portions of MVpc at all levels. Labeling involved large multipolar cells (Figs 9, and 10C and D). Their distribution was bilateral, with a slight *ipsilateral* dominance, even caudally (Figs 2, 8, 9, and 10C and D).

#### **Reticular formation**

Disynaptic input to LIPv was derived from a substantial number (n=144, approximately half of the numbers of cells labeled after MIP injections) of large multipolar cells in Gi/DPGi (Figs 8, 9 and 10). Their distribution was bilateral, with a *contralateral* dominance, as in the MIP case, but showed different rostrocaudal dominance. Most of the



labeled neurons were concentrated in the rostral medulla (Figs 9G-L and 10A-C), especially in Gi at the level of the VI nucleus and in both DPGi and Gi more caudally, whereas only a few labeled cells were found at caudal medullary levels, mainly in DPGi (Fig. 9A-F). The paramedian tract cell groups were not labeled. As in the MIP case, a few cells were labeled in the dorsal portion of the LRF adjoining the rostral MVmc (Figs 9I-J and 10A, asterisks) and in the LRF near the SpV (Fig. 9C and D).

### **Scarpa's ganglia, vestibular nuclei and reticular formation – trisynaptic inputs to MIP (3 days)**

#### **Vestibular (Scarpa's) ganglia**

At the trisynaptic time point, labeled cells appeared in Scarpa's ganglion on both sides, revealing that MIP receives trisynaptic vestibular inputs directly from the labyrinth via second-order vestibular neurons in the VN (Figs 2 and 11D). Importantly, labeling of Scarpa's ganglia involved a great number of neurons (n= 161 contralaterally and n= 15 ipsilaterally in two series of sections) (Fig. 11D). Cell counts in the ipsilateral (left) Scarpa's ganglion are likely to be a large underestimate of the total population of labeled vestibular ganglion's cells targeting trisynaptically MIP, because much less tissue of the left Scarpa's ganglion was available for analysis (more than half of it was lost during immunohistochemical processing). On both sides, rabies immunolabeling visualized the characteristic round cell bodies of vestibular ganglion cells, some intensely labeled and others weakly labeled, intermingled with many unlabeled cells; axons were not labeled (Fig. 11D).

Some labeled cells were also found bilaterally in the interstitial nucleus of the vestibular nerve (Langer *et al.*, 1985; Newlands *et al.*, 2003) (Figs 11A and 12I). At the trisynaptic time point, there was a major increase in the number and distribution of labeled neurons in the brainstem (see below, Figs 11 and 12), which could reflect the visualization of inputs to cortical areas directly connected with MIP and to brainstem and cerebellar populations targeting MIP (for the cerebellar results, see Prevosto *et al.*, 2010). Thus, the heavy (mirror-image) direct connections between homotopic MIP portions of the two hemispheres (Figs 3C, D and F, and 4) and the resulting disynaptic labeling in the contralateral thalamus (Figs 2 and 5) likely contribute to explain why labeling in the VN (and MRF) became more bilateral at the trisynaptic time point (Fig. 12). The increase in labeling of VN and MRF at this time point may also be mediated by heavy commissural pathways between the VN, as well as reciprocal vestibulo-reticular connections and reticulo-reticular connections along the rostrocaudal axis (Graybiel, 1977; Corvaja *et al.*, 1979; Matsuyama *et al.*, 1988; Cowie *et al.*, 1994). Thus, the relative contribution of each pathway to the trisynaptic labeling described below could not be precisely determined.

### **Vestibular nuclei**

In the vestibular complex, labeling became more bilateral and involved a much greater number of neurons on both sides in MV, SV, DV and Y group (Figs 11 and 12). The increase in cell number and distribution was particularly pronounced in the MV, where labeling at 3 days included also its caudal pole (Fig. 12). Even at this time point, labeling was particularly pronounced contralaterally in MVmc and lateral MVpc (where labeled neurons were found at the disynaptic time point), where it included a dense network of labeled cell processes (Fig. 11C, E and F) (unlike other VN regions where labeling was initial, Fig. 11). Labeling additionally involved a substantial number of neurons in more medial portions of

MVpc at all levels, but the dorsomedial portion of MVpc and the marginal zone near the PH remained unlabeled at most levels (Figs 11 and 12). A substantial increase in the number and distribution of labeled cells occurred also in the DV (especially ventrally), SV and Y groups, whereas the large vestibulospinal neurons in the LV nuclei remained unlabeled (Figs 11 and 12).

### **Reticular formation**

A major increase in the number and distribution of labeled neurons occurred in the MRF on both sides (Figs 11 and 12). Labeling in DPGi became more extensive, still showing a clear contralateral dominance at most levels, but a bilateral distribution at the level of the VI nucleus. Notably, labeled cells were present throughout the Gi, including ventral portions which were unlabeled at the disynaptic time point (Figs 11A-C, E and G-I, and 12). At this time point, labeling clearly delineated the entire morphology of MRF neurons, including distal cell processes extending into the medial longitudinal fasciculus (Fig. 11B, E and G-I). A substantial increase in the number of labeled neurons also occurred in the dorsal LRF near the rostral MVmc (Figs 11A and 12I-K). Most of the other LRF portions remained unlabeled, with the exception of some cells around the facial nucleus, near the SpV (Fig. 12) and in the vicinity of the lateral reticular nucleus, where a large number of labeled cells were found at 3 days, mostly contralaterally (Fig. 12A-C). Some inferior olive portions were also labeled.

## **DISCUSSION**

The present study provides the first description of ascending polysynaptic pathways that convey vestibular signals to rostral MIP and LIPv. In addition to direct projections from ‘vestibular’ cortical areas (Prevosto *et al.*, 2011), we found that these PPC areas receive bilateral disynaptic pathways from the VN, which strongly target rostral MIP and provide

minor inputs to LIPv. We also demonstrate that rostral MIP receives vestibular inputs from the labyrinth vestibular end organs via a trisynaptic pathway (Figs 2 and 13A), as directly as classical “vestibular cortical areas” (Fukushima, 1997; Lopez & Blanke, 2011).

We also show that rostral MIP and LIPv receive ascending disynaptic pathways from the dorsal medullary MRF (Figs 2 and 13), which target most prominently MIP and provide a topographically distinct input to LIPv. These hitherto unknown pathways are suited to carry an efference copy of arm and head movement commands, because they originate from MRF reticulospinal regions that belong to reaching and head movement networks. These findings have important implications for the understanding of the influence of vestibular information and efference copy signals on rapid updating of internal representations and reference frame transformations, and internal models for action in the PPC.

### **Vestibular and reticulothalamic pathways to LIPv: potential neural basis of head gain fields.**

LIPv is part of the ‘parietal eye field’ which participates in visuospatial processing and saccade encoding (Buneo & Andersen, 2006; Bisley & Goldberg, 2010). We show that LIPv receives substantial disynaptic pathways from the rostral MRF (Gi/DPGi) (approximately half of the number of cells targeting rostral MIP) (Figs 8, 9 and 10). Conversely, disynaptic pathways from the VN are minor, and originate bilaterally from the same MV portions that target MIP (Figs 8, 9 and 10). Their functional significance will be discussed in the MIP section. The stronger vestibular inputs to MIP versus LIPv suggests greater relevance of vestibular signals for extrapersonal space representations and arm movement planning exerted by MIP, versus eye movements and gaze-related functions of LIP.

Both vestibulo- and reticulothalamic pathways are routed to LIPv mainly via the central thalamus (CL and lateral MD) (see Results). Thalamo-cortical pathways through the central thalamus transmit eye position and velocity signals to LIPv and MIP from the PH (Prevosto *et al.*, 2009) (Fig. 13) and corollary discharge/efference copy signals for online monitoring of saccades (Wurtz, 2008; Tanaka & Kunimatsu, 2011).

To discuss the significance of reticulothalamic pathways to LIPv (and MIP), it is important to recall the functional organization of the MRF (Gi/DPGi), from which these pathways originate. There is a crude topography of motor output in the primate MRF, with eye movement-related neurons rostrally and dorsally in DPGi, cells projecting to both eye and neck motor pools at either side of the Gi/DPGi border and in Gi, and reticulospinal cells targeting more caudal spinal segments concentrated mainly more ventrally in Gi (Robinson *et al.*, 1994; Ugolini *et al.*, 2006; Sakai *et al.*, 2009; Fregosi *et al.*, 2017). In stimulation studies, head movements tend to be elicited especially dorsally and rostrally, and proximal arm movements especially at more caudoventral sites (Cowie & Robinson, 1994; Cowie *et al.*, 1994; Quessy & Friedman, 2004).

Reticulo-thalamic pathways to LIPv originate mostly from the rostral part of the ‘reticular head movement region’ (in rostral Gi and at the Gi/DPGi border, at the level of the VI nucleus and neighboring levels) (Fig. 9). Stimulation of this MRF portion consistently evokes ipsilateral head rotation (Cowie & Robinson, 1994; Cowie *et al.*, 1994; Quessy & Friedman, 2004). It has the lowest threshold facilitatory effects on the upper trapezius muscle (a head rotator) (Davidson & Buford, 2006). Because MRF projections are highly collateralized (axons dichotomizing into an ascending and a descending branch, Robertson & Feiner, 1982), it is highly possible that reticulothalamic projections may be collaterals of reticulospinal neurons.

The significance of prominent reticulothalamic pathways to LIPv may be viewed in the context of head position modulation of LIPv activity and a role in planning gaze shifts (Buneo & Andersen, 2006). Importantly, many neurons in LIP are gain modulated by both eye and *head* position, i.e., gaze direction (Brotchie *et al.*, 1995; Andersen *et al.*, 1999).

Theoretically, head gain fields can be derived by the integration of vestibular signals (indicating head orientation in the world), neck proprioceptive signals (indicating head orientation on the body) and efference copy head movement signals (Crowell *et al.*, 1998; Andersen *et al.*, 1999). Our demonstrations that LIPv receives neck proprioceptive inputs disynaptically from the DCN (Prevosto *et al.*, 2011), and prominent disynaptic inputs from the rostral MRF head movement region (putative head efference copy signals), but minor vestibular inputs from the VN (Fig. 13B), are remarkably in keeping with the reports that head position modulation in LIP (Brotchie *et al.*, 1995) is primarily driven by proprioceptive signals and/or efference copy from the head/neck motor system, with little contribution of vestibular signals (Snyder *et al.*, 1998; Andersen *et al.*, 1999; Buneo & Andersen, 2006).

### **Vestibular and reticulothalamic pathways to rostral MIP**

The targeted rostral MIP is an arm movement area (Mountcastle *et al.*, 1975; Kalaska & Crammond, 1992; Johnson *et al.*, 1996), and is part of the functionally defined ‘parietal reach region’, together with caudal MIP and V6A (Andersen *et al.*, 2014).

### **Ascending vestibular pathways to rostral MIP: neural basis for active-passive movement discrimination**

Disynaptic pathways to rostral MIP originate bilaterally (especially contralaterally) from the VN (especially from lateral portions of the MV) (Figs 6, 7 and 8). The bilaterality of these ascending vestibular pathways is in keeping with evidence of bilateral VN projections

to the thalamus (Lang *et al.*, 1979; Büttner & Lang, 1979), and with the reports that most vestibular units in the monkey thalamus can be activated from both labyrinths (Deecke *et al.*, 1977). Neurons in the VN that project to the thalamus are not numerous, and their terminations are sparse and patchy (Lang *et al.*, 1979; Büttner & Lang, 1979; Tracey *et al.*, 1980; Asanuma *et al.*, 1983a; Meng *et al.*, 2007; Marlinski & McCrea, 2009); correspondingly, vestibular units are infrequently encountered in the thalamus (Büttner & Henn, 1976; Liedgren *et al.*, 1976; Büttner *et al.*, 1977; Magnin & Fuchs, 1977; Meng *et al.*, 2007, 2010).

In view of this organization, the high number of labeled neurons in the VN (at the disynaptic time point) (Figs 6, 7 and 8) and Scarpa's ganglia (trisynaptic time point) (Figs 2, 11D and 13A) in the MIP experiments is striking, and suggests that rostral MIP is a major target of vestibulothalamic pathways. The major quantitative differences in disynaptic vestibular inputs to MIP versus LIPv are probably mediated by VN projections to VPLc and VLc, i.e., thalamic nuclei that supply MIP but not LIPv (see Results). The response dynamics of vestibular neurons in the thalamus (Meng *et al.*, 2007; Meng & Angelaki 2010; Dale & Cullen, 2017) are similar to those of eye movements-insensitive neurons in the VN, which include vestibulospinal neurons (Fuchs & Kimm, 1975; McCrea *et al.*, 1999) and are regarded as the source of vestibulothalamic pathways (Angelaki & Cullen, 2008; Cullen, 2012). Approximately 10% of vestibulothalamic neurons were shown to be vestibulospinal neurons (Meng *et al.*, 2001).

Vestibular signals are important to distinguish self-generated (active) from externally induced (passive) movement. Discrimination between active and passive body motion is crucial for self-motion perception and effective motor actions (Cullen, 2012; Laurens & Angelaki, 2017). Unlike vestibular responses to passive motion (Lopez & Blanke, 2011), the cortical processing of active self-motion has not been widely studied. To date, a single study

has compared vestibular responses to active and passive self-motion, in the targeted rostral MIP and neighboring VIP (Klam & Graf, 2006). In both areas, a population of neurons distinguished between active and passive head movements. During active movement, vestibular responses were diminished (or extinguished) in the majority of neurons (Klam & Graf, 2006).

The prominent ascending vestibular pathways to rostral MIP revealed here can explain the distinction between active and passive movements in rostral MIP, because a similar distinction has been demonstrated in vestibular neurons in the ventral posterior lateral thalamus (Dale & Cullen, 2017) and VN (Roy & Cullen, 2001, 2004; Carriot *et al.*, 2013; Brooks & Cullen, 2014) including both vestibulothalamic (Marlinksy & McCrea, 2009) and vestibulospinal neurons (McCrea *et al.*, 1999). Specifically, their vestibular responses are markedly reduced during active movements; responses attenuation occurs only when the sensory consequences of motion (proprioceptors activation) match the motor-generated expectation (Roy & Cullen, 2004; Cullen 2012; Carriot *et al.*, 2013; Brooks & Cullen, 2014; Dale & Cullen, 2017). This has been demonstrated in both unimodal (vestibular) and bimodal (vestibulo-proprioceptive) neurons, which respectively encode head and body motion (Marlinski & McCrea, 2008, 2009; Dale & Cullen, 2017).

Vestibular pathways to rostral MIP potentially provide a major correlate for fast updating of self-motion estimates, for online changes of reference frame representation from egocentric (during passive movement) to allocentric (during active movement), and driving motor corrections (see Functional considerations). Because of the reciprocal connections between MIP and VIP (Fig. 3C and E; Lewis & Van Essen, 2000b; Bakola *et al.*, 2017), ascending vestibular inputs to MIP likely influence VIP vestibular properties as well.



## **Reticulo-thalamic pathways to MIP: putative efference copy pathways of head and arm movements commands.**

Disynaptic pathways from the medullary MRF prominently originate from both the rostral MRF (also targeting LIPv) and from more caudal MRF portions (which have limited inputs to LIPv) (Figs 6, 7, 8 and 13), where head and arm movements or facilitatory effects can be evoked by stimulation (Cowie & Robinson, 1994; Davidson & Buford, 2006). Stronger MRF inputs may be mediated by reticulothalamic projections to VPLc and caudal VLc, which supply MIP but not LIPv (see Results).

In addition to head movements, the labelled MRF regions are part of a tightly interconnected circuit for control of reaching, together with rostral MIP and other SPL reach areas and related frontal lobe motor areas, the superior colliculus (SC) and the cerebellar interpositus, which heavily targets MIP disynaptically (Prevosto *et al.*, 2010) (Fig. 13A). Indeed, these MRF reticulospinal domains (part of the classic ‘medial descending pathways’, Lawrence & Kuypers, 1968a,b; Kuypers, 1981) have activity related to arm movement preparation and performance of reaching (Buford & Davidson, 2004) and output effects in shoulder, arm and forearm muscles (Davidson & Buford, 2004, 2006; Davidson *et al.*, 2007).

In addition to crossed projections from the SC (Harting, 1977; May, 2006) and the cerebellar nuclei (Batton *et al.*, 1977; Asanuma *et al.*, 1983b) (Fig. 13), the labeled MRF receives major bilateral projections from all frontal lobe motor areas (Kuypers, 1960, 1981; Kuypers & Lawrence 1967; Catsman-Berrevoets & Kuypers, 1976; Keizer & Kuypers, 1989). Many such projections are collaterals of corticospinal fibers, notably issued by dorsal premotor cortex (PMd) arm areas (F2 dimple region, ventrorostral F2) (Keizer & Kuypers, 1989) belonging to the parieto-frontal circuits encoding reach-to-grasp actions, which are

heavily interconnected with rostral and caudal MIP and V6A (Matelli *et al.*, 1988; Distler & Hoffmann, 2015; Bakola *et al.*, 2017; Galletti & Fattori, 2018), i.e., with the entire parietal reach region.

Controlling goal-directed arm movements is challenging, because it requires coordinating the recruitment of many muscles acting on multiple joints. Growing evidence suggests that the CNS simplifies this control through motor ‘primitives’ (Overduin *et al.*, 2015). The MRF has a major role in muscle synergies recruitment because MRF reticulospinal pathways branch extensively in medial motor pools and in the ventromedial spinal intermediate zone (Kuypers *et al.*, 1962), which has the required connectivity to mediate wide synergies involving arm, shoulder and axial muscles (Kuypers, 1981). Importantly, the role of the MRF in mediating visually guided reaching and a gating effect of frontal lobe motor areas on its activity was already revealed in classic behavioral studies after lesion (Lawrence & Kuypers, 1968a,b; Moll & Kuypers, 1977).

Subcortical drive to the MRF for reach and gaze activity is provided by crossed tecto-reticulospinal pathways (Harting, 1977; May, 2006), which originate from the caudal SC intermediate and deep layers (Cowie *et al.*, 1994). Reach neurons have been identified in these layers (Kutz *et al.*, 1997; Werner *et al.*, 1997a,b; Stuphorn *et al.*, 1999, 2000; Philipp & Hoffmann, 2014), which receive projections from multiple cortical areas, including M1 and PMd arm areas (Distler & Hoffmann, 2015) and MIP (Lynch *et al.*, 1985).

In view of these properties and connectivity, disynaptic pathways from the MRF to rostral MIP would have the required characteristic to convey efference copy signals potentially reflecting the combined activity of the same frontal cortical and subcortical reach

networks through which rostral MIP and the other arm-related regions of the PCC exert their command operations. They could also transmit head signals (see discussion of LIPv results).

Their contribution to internal models for action in the PPC would clearly deserve to be investigated in functional studies.

### **Functional considerations**

#### **Role of ascending vestibular pathways and MRF efference copy signals to rostral MIP in self-motion computation and internal models for online control of arm movements**

Our findings have potential implications for the understanding of movement planning and online control operations of the PPC. Together with the other SPL arm areas, MIP acts as a sensorimotor interface for planning and online control of goal-directed arm movements (Mountcastle *et al.*, 1975; Buneo & Andersen, 2006; Andersen *et al.*, 2014). In humans, lesions of the SPL or restricted to the medial bank of the IPS (Trillenber *et al.*, 2007) cause optic ataxia, a major impairment in sensorimotor guidance of reaching movements (Rossetti *et al.*, 2003; Andersen *et al.*, 2014). Importantly, optic ataxia-like deficits have been reproduced in monkeys with inactivation targeting rostral MIP (Hwang *et al.*, 2012, 2014), caudal MIP (Yttri *et al.*, 2014), or SPL area PEc (Battaglia-Mayer *et al.*, 2013), or V6A lesion (Battaglini *et al.*, 2002).

Signals from different sensory modalities are aligned into common reference frames for integration (Buneo & Andersen, 2006). Reference frame transformations are implemented already at the level of single neurons in the PPC, so that a cell's response within its visual receptive field, and peripersonal space (PPS) representation, is remapped in function of eye, head, or arm position (gain fields) (Andersen & Buneo, 2002; Blanke *et al.*, 2015).

Multimodal PPC neurons have not only eye-centered or head-centered receptive fields (Galletti *et al.*, 1993; Duhamel *et al.*, 1997) but also mixed or combined receptive fields (Andersen & Buneo, 2002).

Motor plans are continuously updated by internal feedback loops. Considerable evidence points to internal models in the PPC (and cerebellum) that integrate multisensory inflow and efference copy (replicas of motor commands) to enable fast online corrections (Desmurget & Grafton, 2000; Buneo & Andersen, 2006; Mulliken *et al.*, 2008). In addition to fronto-parietal projections (Bakola *et al.*, 2017), efference copy signals of ongoing reaching and head movements could be fed back to the PPC by the ascending MRF pathways to the PPC first demonstrated here (see above), which, theoretically, should also carry the active/passive movement distinction, because the labeled MRF and VN domains are heavily interconnected (Graybiel, 1977; Corvaja *et al.*, 1979; Cowie & Robinson, 1994) and both are major targets of cerebellar output (Batton *et al.*, 1977; Asanuma *et al.*, 1983b; Gonzalo-Ruiz & Leichnetz, 1990) (Fig. 13A). Importantly, cerebellar rostral fastigial neurons distinguish between active and passive movements (Brooks & Cullen, 2013; Brooks *et al.*, 2015) and similar properties were suggested for interpositus neurons (which heavily target rostral MIP) (Fig. 13A) (see Prevosto *et al.*, 2010).

Distinction between active and passive movements in vestibular neurons, and attenuation of vestibular responses during active movement, is similarly explained by internal models, likely implying the cerebellum (see Dale & Cullen, 2017; Laurens & Angelaki, 2017). Ascending vestibular pathways to rostral MIP, demonstrated here, provide a correlate for driving fast motor corrections. Indeed, there is evidence that the brain uses vestibular signals to generate the appropriate reaching command required to maintain accuracy during

self-motion (Moreau-Debord *et al.*, 2014; Blouin *et al.*, 2015). Reach corrections to vestibular perturbations are task-dependent, consistent with online integration of self-motion signals into an internal model for reach control (Keyser *et al.*, 2017). TMS studies point to a key role of an intermediate portion of the human medial IPS for online adjustments of goal-directed arm movements based on vestibular and proprioceptive feedback (Reichenbach *et al.*, 2014, 2016). Our demonstrations that rostral MIP receives, via parallel pathways, arm/shoulder proprioceptive inputs from the DCN (Prevosto *et al.*, 2011), prominent vestibular signals from the VN and labyrinths, reach-related MRF efference copy pathways (present findings), and major output channels from arm movement-related cerebellar domains (Prevosto *et al.*, 2010) reveal the underlying anatomical substrates (see Fig. 13A).

The vestibular and reticular pathways to rostral MIP investigated in the present study may also contribute to the properties of more caudal portions of the ‘parietal reach region’ (caudal MIP and V6A) and SPL area PEc (Buneo & Andersen, 2006; Andersen *et al.*, 2014; Galletti & Fattori, 2018) because rostral MIP heavily projects to these areas (Caminiti *et al.*, 1999; Bakola *et al.*, 2010, 2017). Functional data suggest that PPC reach-related areas may not be functionally equivalent, and rostral MIP may have a more substantial and/or direct role in vestibular and proprioceptive processing for arm movement guidance and eye/hand coordination coupling (Hwang *et al.*, 2012, 2014; Battaglia-Mayer *et al.*, 2013; Yttri *et al.*, 2014; Reichenbach *et al.*, 2014, 2016). Rostral (but not caudal) MIP may also influence proprioceptive inflow to the PPC, because it projects to the proprioceptive DCN domains (Kuypers, 1960; Catsman-Berrevoetz & Kuypers, 1976) from where disynaptic pathways to rostral MIP originate (see Prevosto *et al.*, 2011) (Fig. 13A).

## **Vestibular contribution to body schema and to the sense of ownership**

The PPC plays a major role in multisensory integration which is crucial for establishing and maintaining a ‘body schema’, defined as an action-oriented, sensorimotor body representation (Maravita & Iriki, 2004; Giummarra *et al.*, 2008; Blanke *et al.*, 2015). Damage to the PPC can cause a variety of disorders of bodily self-consciousness, which can affect body ownership, embodiment and/or spatial awareness (Vallar, 1998; Danckert & Ferber, 2006; Lopez *et al.*, 2008; Blanke, 2012). The importance of vestibular processing in maintaining self-identification is exemplified by the reports that limb ownership in asomatognosia and somatoparaphrenia can be restored using caloric vestibular stimulation (Bisiach *et al.*, 1991; Giummarra *et al.*, 2008; Spitoni *et al.*, 2016), and that vestibular stimulation is effective for neglect rehabilitation (Vallar 1998; Kerkhoff & Schenck, 2012).

Illusory states of bodily self-consciousness can also be induced experimentally by manipulating multisensory inputs, eliciting visuovestibular or visuotactile conflicts (Blanke, 2012; Blanke *et al.*, 2015). Illusory self-attribution of a rubber hand is induced by synchronous tactile stimulation of the visible fake hand and of the (hidden) real hand (Blanke *et al.*, 2015). Interestingly, brief, low-intensity, galvanic vestibular stimulation, which induces vestibular activations similar to those of natural movement, significantly lowers the proprioceptive drift towards the fake hand perceived during this illusion, suggesting that vestibular inputs influence the multisensory weighting underlying bodily awareness (Ferrè *et al.*, 2015). This process is likely based on the mechanisms, demonstrated in multisensory MIP/ area 5 neurons, which reshape PPS and mediate incorporation of external objects (e.g., tools, prosthesis) in the body representation (Graziano *et al.*, 2000; Maravita & Iriki, 2004; Blanke *et al.*, 2015).

## **Acknowledgements**

This work was supported by the European Union Grant EU 5th FP (QLRT-2001-00151, EUROKINESIS) and the Centre National de la Recherche Scientifique.

## **Competing interests**

The authors declare that they have no conflict of interest.

## **Author contributions**

GU designed study, conducted the experiments, collected data, analyzed data, wrote the paper. VP collected data, analyzed data, edited the paper. WG designed study, conducted the experiments, collected data, edited the paper.

## **Data accessibility**

Raw data and materials are not made publicly available for lack of institutional plan or support to do so in any comprehensive manner. Raw data and materials are archived by GU.

Requests for data sharing may be addressed to that author.

## **Abbreviations**

APul, anterior pulvinar nucleus; CL, central lateral nucleus; CM, central median nucleus; CTB, cholera toxin B; CuT, cuneate nucleus, pars triangularis; das, dorsal accessory stria; DCN, dorsal column nuclei; DPGi, dorsal paragigantocellular reticular formation; DV, descending vestibular nucleus; ECu, external cuneate nucleus; fr, fasciculus retroflexus; g, genu of the facial nerve; Gi, gigantocellular reticular formation; Hb, habenula; icp, inferior

cerebellar peduncle; III, oculomotor nucleus; InVIIIIn, interstitial nucleus of the vestibular nerve; IO, inferior olive; IPS, intraparietal sulcus; IPul, inferior pulvinar nucleus; LD, lateral dorsal nucleus; LG, lateral geniculate nucleus; LIPd, lateral intraparietal area, dorsal; LIPv, lateral intraparietal area, ventral; LP, lateralis posterior nucleus; LV, lateral vestibular nucleus; MD, medial dorsal nucleus; M1, primary motor cortex; MG, medial geniculate nucleus; MIP, medial intraparietal area; mlf, medial longitudinal fasciculus; MRF, medial reticular formation; MV, medial vestibular nucleus; MVmc, medial vestibular nucleus, magnocellular; MVpc, medial vestibular nucleus, parvocellular; LRF, lateral reticular formation; LRN, lateral reticular nucleus; Nst, nucleus of the solitary tract; PH, prepositus hypoglossi; PMd, premotor cortex, dorsal; PPC, posterior parietal cortex; PPS, peripersonal space; pt, pyramidal tract; Rt, reticular thalamic nucleus; SC, superior colliculus; scp, superior cerebellar peduncle; SG, suprageniculate nucleus; SPL, superior parietal lobe; SpV, spinal trigeminal nucleus; SV, superior vestibular nucleus; VI, abducens nucleus; VII, facial nucleus; VIIIn, facial nerve (descending limb); VIIIIn, vestibular nerve; VIP, ventral intraparietal area; VLc, ventral lateral nucleus, pars caudalis; VLG, ventral lateral geniculate nucleus; VLps, ventral lateral nucleus, pars postrema; VN, vestibular nuclei; VPI, ventral posterior inferior nucleus; VPLc, ventral posterior lateral nucleus, pars caudalis; VPLo, ventral posterior lateral nucleus, pars oralis; VPM, ventral posterior medial nucleus; XII, hypoglossal nucleus; Y, vestibular Y group; ZI, zona incerta.



## References

- Andersen, R.A. (1997) Multimodal integration for the representation of space in the posterior parietal cortex. *Philos. Trans. R. Soc. Lond., B, Biol. Sci.*, **352**, 1421-1428.
- Andersen, R.A. & Buneo, C.A. (2002) Intentional maps in posterior parietal cortex. *Annu. Rev. Neurosci.*, **25**, 189-220.
- Andersen, R.A., Shenoy, K.V., Snyder, L.H., Bradley, D.C. & Crowell, J.A. (1999) The contributions of vestibular signals to the representations of space in the posterior parietal cortex. *Ann. N. Y. Acad. Sci.*, **871**, 282-292.
- Andersen, R.A., Andersen, K.N., Hwang, E.J. & Hauschild, M. (2014) Optic ataxia: from Balint's syndrome to the parietal reach region. *Neuron*, **81**, 967-983.
- Angelaki, D.E. & Cullen, K.E. (2008) Vestibular system: the many facets of a multimodal sense. *Annu. Rev. Neurosci.*, **31**, 125-150.
- Asanuma, C., Thach, W.T. & Jones, E.G. (1983a) Distribution of cerebellar terminations and their relation to other afferent terminations in the ventral lateral thalamic region of the monkey. *Brain Res.*, **286**, 237-265.
- Asanuma, C., Thach, W.T. & Jones, E.G. (1983b) Brainstem and spinal projections of the deep cerebellar nuclei in the monkey, with observations on the brainstem projections of the dorsal column nuclei. *Brain Res.*, **286**, 299-322.
- Bakola, S., Gamberini, M., Passarelli, L., Fattori, P. & Galletti, C. (2010) Cortical Connections of Parietal Field PEc in the Macaque: Linking Vision and Somatic Sensation for the Control of Limb Action. *Cereb. Cortex*, **20**, 2592-2560.
- Bakola, S., Passarelli, L., Huynh, T., Impieri, D., Worthy, K.H., Fattori, P., Galletti, C., Burman, K.J. & Rosa M.G.P. (2017) Cortical Afferents and Myeloarchitecture Distinguish the Medial Intraparietal Area (MIP) from Neighboring Subdivisions of the Macaque Cortex. *eNeuro*. **4(6)**. pii: ENEURO.0344-17.2017. doi:

- Battaglia-Mayer, A., Ferrari-Toniolo, S., Visco-Comandini, F., Archambault, P.S., Saberi-Moghadam, S. & Caminiti, R. (2013) Impairment of online control of hand and eye movements in a monkey model of optic ataxia. *Cereb. Cortex*, **23**, 2644-2656.
- Battaglini, P.P., Muzur, A., Galletti, C., Skrap, M., Brovelli, A. & Fattori, P. (2002) Effects of lesions to area V6A in monkeys. *Exp. Brain Res.*, **144**, 419-422.
- Batton, R.R. 3rd, Jayaraman, A., Ruggiero, D. & Carpenter, M.B. (1977) Fastigial efferent projections in the monkey: an autoradiographic study. *J. Comp. Neurol.*, **174**, 281-305.
- Ben Hamed, S., Duhamel, J.R., Bremmer, F. & Graf, W. (2001) Representation of the visual field in the lateral intraparietal area of macaque monkeys: a quantitative receptive field analysis. *Exp. Brain Res.*, **140**, 127-144.
- Bisiach, E., Rusconi, M.L. & Vallar, G. (1991) Remission of somatoparaphrenic delusion through vestibular stimulation. *Neuropsychologia*, **29**, 1029-1031.
- Bisley, J.W. & Goldberg, M.E. (2010) Attention, intention, and priority in the parietal lobe. *Annu. Rev. Neurosci.*, **33**, 1-21.
- Blanke, O. (2012) Multisensory brain mechanisms of bodily self-consciousness. *Nat. Rev. Neurosci.*, **13**, 556-571.
- Blanke, O., Slater, M. & Serino, A. (2015) Behavioral, Neural, and Computational Principles of Bodily Self-Consciousness. *Neuron*, **88**, 145-166.
- Blatt, G.J., Andersen, R.A. & Stoner, G.R. (1990) Visual receptive field organization and cortico-cortical connections of the lateral intraparietal area (area LIP) in the macaque. *J. Comp. Neurol.*, **299**, 421-445.
- Blouin, J., Bresciani, J.P., Guillaud, E. & Simoneau, M. (2015) Prediction in the Vestibular Control of Arm Movements. *Multisens. Res.*, **28**, 487-505.

Bremmer, F., Schlack, A., Duhamel, J.R., Graf, W. & Fink, G.R., (2001) Space coding in primate posterior parietal cortex. *Neuroimage*, **14**, S46–S51.

Bremmer, F., Klam, F., Duhamel, J.R., Ben Hamed, S. & Graf, W. (2002) Visual–vestibular interactive responses in the macaque ventral intraparietal area (VIP). *Eur. J. Neurosci.*, **16**, 1569–1586.

Brotchie, P.R., Andersen, R.A., Snyder, L.H. & Goodman, S.J. (1995) Head position signals used by parietal neurons to encode locations of visual stimuli. *Nature*, **375**, 232-235.

Brooks, J.X. & Cullen, K.E. (2009) Multimodal integration in rostral fastigial nucleus provides an estimate of body movement. *J. Neurosci.*, **29**, 10499-10511.

Brooks, J.X. & Cullen, K.E. (2013) The primate cerebellum selectively encodes unexpected self-motion. *Curr. Biol.*, **23**, 947-955.

Brooks, J.X. & Cullen, K.E. (2014) Early vestibular processing does not discriminate active from passive self-motion if there is a discrepancy between predicted and actual proprioceptive feedback. *J. Neurophysiol.*, **111**, 2465-2478.

Brooks, J.X., Carriot, J. & Cullen, K.E. (2015) Learning to expect the unexpected: rapid updating in primate cerebellum during voluntary self-motion. *Nat. Neurosci.*, **18**, 1310-1377.

Buford, J.A. & Davidson, A.G. (2004) Movement-related and preparatory activity in the reticulospinal system of the monkey. *Exp. Brain Res.*, **159**, 284-300.

Buneo, C.A. & Andersen, R.A. (2006) The posterior parietal cortex: sensorimotor interface for the planning and online control of visually guided movements. *Neuropsychologia*, **44**, 2594-2606.

Büttner, U. & Henn, V. (1976) Thalamic unit activity in the alert monkey during natural vestibular stimulation. *Brain Res.*, **103**, 127-132.

Büttner, U., Henn, V. & Oswald, H.P. (1977) Vestibular-related neuronal activity in the

thalamus of the alert monkey during sinusoidal rotation in the dark. *Exp. Brain Res.*, **30**, 435-444.

Büttner, U. & Lang, W. (1979) The vestibulocortical pathway: neurophysiological and anatomical studies in the monkey. *Prog. Brain Res.*, **50**, 581-588.

Caminiti, R., Genovesio, A., Marconi, B., Mayer, A.B., Onorati, P., Ferraina, S., Mitsuda, T., Giannetti, S., Squatrito, S., Maioli, M.G. & Molinari, M. (1999) Early coding of reaching: frontal and parietal association connections of parieto-occipital cortex. *Eur. J. Neurosci.*, **11**, 3339-3345.

Carriot, J., Brooks, J.X. & Cullen, K.E. (2013) Multimodal integration of self-motion cues in the vestibular system: active versus passive translations. *J. Neurosci.*, **33**, 19555-19566.

Catsman-Berrevoets, C.E. & Kuypers, H.G.J.M. (1976) Cells of origin of cortical projections to dorsal column nuclei, spinal cord and bulbar medial reticular formation in the rhesus monkey. *Neurosci. Lett.*, **3**, 245-252.

Chen, A., DeAngelis, G.C. & Angelaki, D.E. (2011) Representation of vestibular and visual cues to self-motion in ventral intraparietal cortex. *J. Neurosci.*, **31**, 12036-12052.

Chen, M., Li, B., Guang, J., Wei, L., Wu, S., Liu, Y. & Zhang M. (2016) Two subdivisions of macaque LIP process visual-oculomotor information differently. *Proc. Natl. Acad. Sci. U.S.A.*, **113**, E6263-E6270.

Colby, C.L. & Duhamel, J.R. (1991) Heterogeneity of extrastriate visual areas and multiple parietal areas in the macaque monkey. *Neuropsychologia*, **29**, 517-537.

Colby, C.L., Gattass, R., Olson, C.R. & Gross, C.G. (1988) Topographical organization of cortical afferents to extrastriate visual area PO in the macaque: a dual tracer study. *J. Comp. Neurol.*, **269**, 392-413.

Corvaja, N., Mergner, T. & Pompeiano O. (1979) Organization of reticular projections to the

vestibular nuclei in the cat. *Prog. Brain Res.*, **50**, 631-644.

Cowie, R.J. & Robinson, D.L. (1994) Subcortical contributions to head movements in macaques. I. Contrasting effects of electrical stimulation of a medial pontomedullary region and the superior colliculus. *J. Neurophysiol.*, **72**, 2648-2664.

Cowie, R.J., Smith, M.K. & Robinson, D.L. (1994) Subcortical contributions to head movements in macaques. II. Connections of a medial pontomedullary head-movement region. *J. Neurophysiol.*, **72**, 2665-2682.

Crowell, J.A., Banks, M.S., Shenoy, K.V. & Andersen, R.A. (1998) Visual self-motion perception during head turns. *Nat. Neurosci.*, **1**, 732-737.

Cullen, K.E. (2012) The vestibular system: multimodal integration and encoding of self-motion for motor control. *Trends Neurosci.*, **35**, 185-196.

Dale, A. & Cullen, K.E. (2017) The Ventral Posterior Lateral Thalamus Preferentially Encodes Externally Applied Versus Active Movement: Implications for Self-Motion Perception. *Cereb. Cortex*, **28**, 1-14.

Danckert, J. & Ferber, S. (2006) Revisiting unilateral neglect. *Neuropsychologia*, **44**, 987-1006.

Davidson, A.G. & Buford, J.A. (2004) Motor outputs from the primate reticular formation to shoulder muscles as revealed by stimulus-triggered averaging. *J. Neurophysiol.*, **92**, 83-95.

Davidson, A.G. & Buford, J.A. (2006) Bilateral actions of the reticulospinal tract on arm and shoulder muscles in the monkey: stimulus triggered averaging. *Exp. Brain Res.*, **173**, 25-39.

Davidson, A.G., Schieber, M.H. & Buford, J.A. (2007) Bilateral spike-triggered average effects in arm and shoulder muscles from the monkey pontomedullary reticular formation. *J. Neurosci.*, **27**, 8053-8058.

- Deecke, L., Schwarz, D.W. & Fredrickson, J.M. (1977) Vestibular responses in the rhesus monkey ventroposterior thalamus. II. Vestibulo-proprioceptive convergence at thalamic neurons. *Exp. Brain Res.*, **30**, 219-232.
- Desmurget, M. & Grafton, S. (2000) Forward modeling allows feedback control for fast reaching movements. *Trends Cogn. Sci.*, **4**, 423-431.
- Distler, C. & Hoffmann, K.P. (2015) Direct projections from the dorsal premotor cortex to the superior colliculus in the macaque (*macaca mulatta*). *J. Comp. Neurol.*, **523**, 2390-2408.
- Duhamel, J.R., Bremmer, F., Ben Hamed, S. & Graf, W. (1997) Spatial invariance of visual receptive fields in parietal cortex neurons. *Nature*. **389**, 845-848.
- Ferrè, E.R., Berlot, E. & Haggard, P. (2015) Vestibular contributions to a right-hemisphere network for bodily awareness: combining galvanic vestibular stimulation and the "Rubber Hand Illusion". *Neuropsychologia*, **69**, 140-147.
- Filimon, F., Nelson, J.D., Huang, R.S. & Sereno, M.I. (2009) Multiple parietal reach regions in humans: cortical representations for visual and proprioceptive feedback during on-line reaching. *J. Neurosci.*, **29**, 2961-2971.
- Fregosi, M., Contestabile, A., Hamadjida, A. & Rouiller, E.M. (2017) Corticobulbar projections from distinct motor cortical areas to the reticular formation in macaque monkeys. *Eur. J. Neurosci.*, **45**, 1379-1395.
- Fuchs, A.F. & Kimm, J. (1975) Unit activity in vestibular nucleus of the alert monkey during horizontal angular acceleration and eye movement. *J. Neurophysiol.*, **38**, 1140-1161.
- Fukushima K. (1997) Corticovestibular interactions: anatomy, electrophysiology, and functional considerations. *Exp. Brain Res.*, **117**, 1-16.
- Galletti, C. & Fattori, P. (2018) The dorsal visual stream revisited: Stable circuits or dynamic pathways? *Cortex*, **98**, 203-217.

Galletti, C., Battaglini, P.P. & Fattori, P. (1993) Parietal neurons encoding spatial locations in craniotopic coordinates. *Exp Brain Res.* **96**, 221-229.

Giummarra, M.J., Gibson, S.J., Georgiou-Karistianis, N. & Bradshaw, J.L. (2008) Mechanisms underlying embodiment, disembodiment and loss of embodiment. *Neurosci. Biobehav. Rev.*, **32**, 143-160.

Gonzalo-Ruiz, A & Leichnetz, G.R. (1990) Connections of the caudal cerebellar interpositus complex in a new world monkey (*Cebus apella*). *Brain Res Bull.* **25**, 919-927.

Graybiel, A.M. (1977) Direct and indirect preoculomotor pathways of the brainstem: an autoradiographic study of the pontine reticular formation in the cat. *J. Comp. Neurol.*, **175**, 37-78.

Graziano, M.S., Cooke, D.F. & Taylor, C.S. (2000) Coding the location of the arm by sight. *Science*, **290**, 1782-1786.

Grefkes, C., Ritzl, A., Zilles, K. & Fink, G.R. (2004) Human medial intraparietal cortex subserves visuomotor coordinate transformation. *Neuroimage*, **23**, 1494-1506.

Harting, J.K. (1977) Descending pathways from the superior colliculus: an autoradiographic analysis in the rhesus monkey (*Macaca mulatta*). *J. Comp. Neurol.*, **173**, 583-612.

Hwang, E.J., Hauschild, M., Wilke, M. & Andersen, R.A. (2012) Inactivation of the parietal reach region causes optic ataxia, impairing reaches but not saccades. *Neuron*, **76**, 1021-1029.

Hwang, E.J., Hauschild, M., Wilke, M. & Andersen, R.A. (2014) Spatial and temporal eye-hand coordination relies on the parietal reach region. *J Neurosci.*, **34**, 12884-12892.

Iriki, A., Tanaka, M. & Iwamura, Y. (1996) Coding of modified body schema during tool use by macaque postcentral neurones. *Neuroreport*, **7**, 2325-2330.

Johnson, P.B., Ferraina, S., Bianchi, L. & Caminiti, R. (1996) Cortical networks for visual reaching: physiological and anatomical organization of frontal and parietal lobe arm

regions. *Cereb. Cortex*, **6**, 102-119.

Kalaska, J.F. & Crammond, D.J. (1992) Cerebral cortical mechanisms of reaching movements. *Science*, **255**, 1517-1523.

Keizer, K. & Kuypers, H.G.J.M. (1989) Distribution of corticospinal neurons with collaterals to the lower brain stem reticular formation in monkey (*Macaca fascicularis*). *Exp. Brain Res.*, **74**, 311-318.

Kerkhoff, G. & Schenk, T. (2012) Rehabilitation of neglect: an update. *Neuropsychologia*, **50**, 1072-1079.

Keyser, J., Medendorp, W.P. & Selen, L.P.J. (2017) Task-dependent vestibular feedback responses in reaching. *J. Neurophysiol.*, **118**, 84-92.

Klam, F. & Graf, W. (2003) Vestibular response kinematics in posterior parietal cortex neurons of macaque monkeys. *Eur. J. Neurosci.*, **18**, 995-1010.

Klam, F. & Graf, W. (2006) Discrimination between active and passive head movements by macaque ventral and medial intraparietal cortex neurons. *J. Physiol.*, **274**, 367-386.

Kutz, D.F., Dannenberg, S., Werner, W., Hoffmann, K-P. (1997) Population coding of arm-movement-related neurons in and below the superior colliculus of *Macaca mulatta*. *Biol. Cybern.*, **76**, 331-337.

Kuypers, H.G.J.M. (1960) Central cortical projections to motor and somato-sensory cell groups. An experimental study in the rhesus monkey. *Brain*, **83**, 161-184.

Kuypers, H.G.J.M (1981) Anatomy of the descending pathways. In: Brooks, V., (ed), *Handbook of physiology, Section 1. Neurophysiology, Vol. II, Part 1*. American Physiology Society, Bethesda, Md., pp. 597-666.

Kuypers, H.G.J.M. & Lawrence, D.G. (1967) Cortical projections to the red nucleus and the brain stem in the Rhesus monkey. *Brain Res.*, **4**, 151-88.

Kuypers, H.G.J.M., Fleming, W.R. & Farinholt, J.W (1962) Subcorticospinal projections in



the rhesus monkey. *J. Comp. Neurol.*, **118**, 107-137.

Lang, W., Büttner-Ennever, J.A. & Büttner, U. (1979) Vestibular projections to the monkey thalamus: an autoradiographic study. *Brain Res.*, **177**, 3-17.

Langer, T., Fuchs, A.F., Chubb, M.C., Scudder, C.A. & Lisberger, S.G. (1985) Floccular efferents in the rhesus macaque as revealed by autoradiography and horseradish peroxidase. *J. Comp. Neurol.*, **235**, 26-37.

Langer, T., Kaneko, C.R., Scudder, C.A. & Fuchs, A.F. (1986) Afferents to the abducens nucleus in the monkey and cat. *J. Comp. Neurol.*, **245**, 379-400.

Laurens, J. & Angelaki, D.E. (2017) A unified internal model theory to resolve the paradox of active versus passive self-motion sensation. *Elife*, Oct 18;6. pii: e28074. doi: 10.7554/eLife.28074.

Lawrence, D.G. & Kuypers, H.G.J.M (1968a) The functional organization of the motor system in the monkey. I. The effects of bilateral pyramidal lesions. *Brain*, **91**, 1-14.

Lawrence, D.G. & Kuypers, H.G.J.M. (1968b) The functional organization of the motor system in the monkey. II. The effects of lesions of the descending brain-stem pathways. *Brain*, **91**, 15-36.

Lewis, J.W. & Van Essen, D.C. (2000a) Mapping of architectonic subdivisions in the macaque monkey, with emphasis on parieto-occipital cortex. *J. Comp. Neurol.*, **428**, 79-111.

Lewis, J.W. & Van Essen, D.C. (2000b) Corticocortical connections of visual, sensorimotor, and multimodal processing areas in the parietal lobe of the macaque monkey. *J. Comp. Neurol.*, **428**, 112-137.

Liedgren, S.R., Milne, A.C., Schwarz, D.W. & Tomlinson, R.D. (1976) Representation of vestibular afferents in somatosensory thalamic nuclei of the squirrel monkey (*Saimiri sciureus*). *J. Neurophysiol.*, **39**, 601-612.

Liu, Y., Yttri, E.A. & Snyder, L.H. (2010) Intention and attention: different functional roles for LIPd and LIPv. *Nat. Neurosci.*, **13**, 495-500.

Lopez, C. & Blanke, O. (2011) The thalamocortical vestibular system in animals and humans. *Brain Res. Rev.*, **67**, 119-146.

Lopez, C., Halje, P. & Blanke, O. (2008) Body ownership and embodiment: vestibular and multisensory mechanisms. *Neurophysiol. Clin.*, **38**, 149-161.

Lynch, J.C., Graybiel, A.M. & Lobeck, L.J. (1985) The differential projection of two cytoarchitectonic subregions of the inferior parietal lobule of macaque upon the deep layers of the superior colliculus. *J. Comp. Neurol.*, **235**, 241-254.

Magnin, M. & Fuchs, A.F. (1977) Discharge properties of neurons in the monkey thalamus tested with angular acceleration, eye movement and visual stimuli. *Exp. Brain Res.*, **28**, 93-99.

Maravita, A. & Iriki, A. (2004) Tools for the body (schema). *Trends Cogn. Sci.*, **8**, 79-86.

Marlinski, V. & McCrea, R.A. (2008) Coding of self-motion signals in ventro-posterior thalamus neurons in the alert squirrel monkey. *Exp. Brain Res.*, **189**, 463-472.

Marlinski, V. & McCrea, R.A. (2009) Self-motion signals in vestibular nuclei neurons projecting to the thalamus in the alert squirrel monkey. *J. Neurophysiol.*, **101**, 1730-1741.

Matelli, M., Govoni, P., Galletti, C., Kutz, D.F. & Luppino, G. (1998) Superior area 6 afferents from the superior parietal lobule in the macaque monkey. *J. Comp. Neurol.*, **402**, 327-352.

Matsuyama, K., Ohta, Y. & Mori, S. (1988) Ascending and descending projections of the nucleus reticularis gigantocellularis in the cat demonstrated by the anterograde neural tracer, Phaseolus vulgaris leucoagglutinin (PHA-L). *Brain Res.*, **460**, 124-141.

May, P.J. (2006) The mammalian superior colliculus: laminar structure and connections.

*Prog. Brain Res.* **151**, 321-378.

- McCrea, R.A., Gdowski, G.T., Boyle, R. & Belton, T. (1999) Firing behavior of vestibular neurons during active and passive head movements: vestibulo-spinal and other non-eye-movement related neurons. *J. Neurophysiol.*, **82**, 416-428.
- Meng, H. & Angelaki, D.E. (2010) Responses of ventral posterior thalamus neurons to three-dimensional vestibular and optic flow stimulation. *J. Neurophysiol.*, **103**, 817-826.
- Meng, H., Bai, R.S., Sato, H., Imagawa, M., Sasaki, M. & Uchino, Y. (2001) Otolith-activated vestibulothalamic neurons in cats. *Exp. Brain Res.*, **141**, 415-24.
- Meng, H., May, P.J., Dickman, J.D. & Angelaki, D.E. (2007) Vestibular signals in primate thalamus: properties and origins. *J. Neurosci.*, **27**, 13590-13602.
- Moll, L. & Kuypers, H.G.J.M. (1977) Premotor cortical ablations in monkeys: contralateral changes in visually guided reaching behavior. *Science*, **198**, 317-319.
- Moreau-Debord, I., Martin, C.Z., Landry, M. & Green, A.M. (2014) Evidence for a reference frame transformation of vestibular signal contributions to voluntary reaching. *J. Neurophysiol.*, **111**, 1903-1919.
- Mountcastle, V.B., Lynch, J.C., Georgopoulos, A., Sakata, H. & Acuna, C. (1975) Posterior parietal association cortex of the monkey: Command functions for operations within extrapersonal space. *J. Neurophysiol.*, **38**, 871-908.
- Mulliken, G.H., Musallam, S. & Andersen, R.A. (2008) Forward estimation of movement state in posterior parietal cortex. *Proc. Natl. Acad. Sci. U.S.A.*, **105**, 8170-8177.
- Nagata, S. (1986) The vestibulothalamic connections in the rat: a morphological analysis using wheat germ agglutinin-horseradish peroxidase. *Brain Res.*, **376**, 57-70.
- Newlands, S.D., Vrabec, J.T., Purcell, I.M., Stewart, C.M., Zimmerman, B.E. & Perachio, A.A. (2003) Central projections of the saccular and utricular nerves in macaques. *J. Comp. Neurol.*, **466**, 31-47.

- Ohtake, T. (1992) Ascending projections from the gigantocellular reticular and dorsal paragigantocellular nuclei of the medulla oblongata in the rat: an anterograde PHA-L tracing study. *Neurosci. Res.*, **14**, 96-116.
- Olszewski, J. (1952) *The thalamus of the Macaca mulatta: an atlas for use with the stereotaxic instrument*. Karger, Basel.
- Overduin, S.A, d'Avella, A., Roh, J., Carmena, J.M. & Bizzi, E. (2015) Representation of Muscle Synergies in the Primate Brain. *J. Neurosci.*, **35**, 12615-12624.
- Paxinos, G., Huang, X.-F., & Toga, A. W. (2000) *The Rhesus Monkey Brain in Stereotaxic Coordinates*. Academic Press, San Diego.
- Philipp, R. & Hoffmann, K-P. (2014) Arm movements induced by electrical microstimulation in the superior colliculus of the macaque monkey. *J. Neurosci.*, **34**, 3350-3363.
- Prevosto, V., Ugolini, G., Isom, S. & Graf, W. (2006) Differences in ascending vestibular, eye position, and somatosensory input to medial (MIP/VIPm) and lateral (VIPI/LIPv) intraparietal areas, revealed by retrograde transneuronal transfer of rabies virus. *Program No. 242.18. 2006 Neuroscience Meeting Planner*. Society for Neuroscience, Atlanta, GA. Online.
- Prevosto, V., Graf, W. & Ugolini, G. (2009) Posterior parietal cortex areas MIP and LIPv receive eye position and velocity inputs via ascending preposito-thalamo-cortical pathways. *Eur. J. Neurosci.*, **30**, 1151-1161.
- Prevosto, V., Graf, W. & Ugolini, G. (2010) Cerebellar inputs to intraparietal cortex areas LIP and MIP: functional frameworks for adaptive control of eye movements, reaching, and arm/eye/head movement coordination. *Cereb. Cortex*, **20**, 214-228.
- Prevosto, V., Graf, W. & Ugolini, G. (2011) Proprioceptive pathways to posterior parietal areas MIP and LIPv from the dorsal column nuclei and the postcentral somatosensory cortex. *Eur. J. Neurosci.*, **33**, 444-460.

- Accepted Article
- Quessy, S. & Freedman, E.G. (2004) Electrical stimulation of rhesus monkey nucleus reticularis gigantocellularis. I. Characteristics of evoked head movements. *Exp. Brain Res.*, **156**, 342-356.
- Reichenbach, A., Thielscher, A., Peer, A., Bühlhoff, H.H. & Bresciani, J.P. (2014) A key region in the human parietal cortex for processing proprioceptive hand feedback during reaching movements. *Neuroimage*, **84**, 615-625.
- Reichenbach, A., Bresciani, J.P., Bühlhoff, H.H. & Thielscher, A. (2016) Reaching with the sixth sense: Vestibular contributions to voluntary motor control in the human right parietal cortex. *Neuroimage*, **124**, 869-875.
- Robertson, R.T & Feiner, A.R. (1982) Diencephalic projections from the pontine reticular formation: autoradiographic studies in the cat. *Brain Res.*, **239**, 3-16.
- Robinson, F.R., Phillips, J.O. & Fuchs, A.F. (1994) Coordination of gaze shifts in primates: brainstem inputs to neck and extraocular motoneuron pools. *J. Comp. Neurol.*, **346**, 43-62.
- Rossetti, Y., Pisella, L. & Vighetto, A. (2003) Optic ataxia revisited: visually guided action versus immediate visuomotor control. *Exp. Brain Res.*, **153**, 171-179.
- Roy, J.E. & Cullen, K.E. (2001) Selective processing of vestibular reafference during self-generated head motion. *J. Neurosci.*, **21**, 2131-2142.
- Roy, J.E. & Cullen, K.E. (2004) Dissociating self-generated from passively applied head motion: neural mechanisms in the vestibular nuclei. *J. Neurosci.*, **24**, 2102-2111.
- Rushworth, M.F., Nixon, P.D. & Passingham, R.E. (1997) Parietal cortex and movement. I. Movement selection and reaching. *Exp. Brain Res.*, **117**, 292-310.
- Russchen, F.T, Amaral, D.G. & Price, J.L. (1987) The afferent input to the magnocellular division of the mediodorsal thalamic nucleus in the monkey, *Macaca fascicularis*. *J. Comp. Neurol.*, **256**, 175-210.

- Sakai, S.T., Davidson, A.G. & Buford, J.A. (2009) Reticulospinal neurons in the pontomedullary reticular formation of the monkey (*Macaca fascicularis*). *Neuroscience*, **163**, 1158-1170.
- Schlack, A., Hoffmann, K.P. & Bremmer, F (2002) Interaction of linear vestibular and visual stimulation in the macaque ventral intraparietal area (VIP). *Eur. J. Neurosci.*, **16**, 1877-1886.
- Snyder, L.H., Grieve, K.L., Brotchie, P. & Andersen, R.A. (1998) Separate body- and world-referenced representations of visual space in parietal cortex. *Nature*, **394**, 887-891.
- Spitoni, G.F., Pireddu, G., Galati, G., Sulpizio, V., Paolucci, S. & Pizzamiglio, L. (2016) Caloric Vestibular Stimulation Reduces Pain and Somatoparaphrenia in a Severe Chronic Central Post-Stroke Pain Patient: A Case Study. *PLoS One*, **11**, e0151213.
- Stuphorn, V., Hoffmann, K-P. & Miller, L.E. (1999) Correlation of primate superior colliculus and reticular formation discharge with proximal limb muscle activity. *J. Neurophysiol.*, **81**, 1978-1982.
- Stuphorn, V. Bauswein, E. & Hoffmann, K-P. (2000) Neurons in the primate superior colliculus coding for arm movements in gaze-related coordinates. *J. Neurophysiol.*, **83**, 1283-1299.
- Tanaka, M. & Kunimatsu, J. (2011) Contribution of the central thalamus to the generation of volitional saccades. *Eur. J. Neurosci.*, **33**, 2046-2057.
- Tracey, D.J., Asanuma, C., Jones, E.G. & Porter, R. (1980) Thalamic relay to motor cortex: afferent pathways from brain stem, cerebellum, and spinal cord in monkeys. *J. Neurophysiol.*, **44**, 532-554.
- Trillenber, P., Sprenger, A., Petersen, D., Kompf, D., Heide, W. & Helmchen, C. (2007) Functional dissociation of saccade and hand reaching control with bilateral lesions of the medial wall of the intraparietal sulcus: implications for optic ataxia. *Neuroimage*,

36 Suppl 2, T69-76.

Ugolini, G. (1995) Specificity of rabies virus as a transneuronal tracer of motor networks: transfer from hypoglossal motoneurons to connected second-order and higher order central nervous system cell groups. *J. Comp. Neurol.*, **356**, 457-480.

Ugolini, G. (2010) Advances in viral transneuronal tracing. *J. Neurosci. Methods*, **194**, 2-20.

Ugolini, G. (2011) Rabies virus as a transneuronal tracer of neuronal connections. *Adv. Virus Res.*, **79**, 165-202.

Ugolini, G., Klam, F., Doldan Dans, M., Dubayle, D., Brandi, A.M., Buttner-Ennever, J. & Graf, W. (2006) Horizontal eye movement networks in primates as revealed by retrograde transneuronal transfer of rabies virus: differences in monosynaptic input to "slow" and "fast" abducens motoneurons. *J. Comp. Neurol.*, **498**, 762-785.

Vallar G (1998) Spatial hemineglect in humans. *Trends Cogn. Sci.*, **2**, 87-97.

Weisberg, J.A. & Rustioni, A. (1977) Cortical cells projecting to the dorsal column nuclei of rhesus monkeys. *Exp. Brain Res.*, **28**, 521-528.

Werner, W., Dannenberg, S. & Hoffmann, K-P. (1997a) Arm-movement-related neurons in the primate superior colliculus and underlying reticular formation: comparison of neuronal activity with EMGs of muscles of the shoulder, arm and trunk during reaching. *Exp. Brain Res.*, **115**, 191-205.

Werner, W., Hoffmann, K-P. & Dannenberg, S. (1997b) Anatomical distribution of arm-movement-related neurons in the primate superior colliculus and underlying reticular formation in comparison with visual and saccadic cells. *Exp. Brain Res.*, **115**, 206-216.

Wurtz, R.H. (2008) Neuronal mechanisms of visual stability. *Vision Res.*, **48**, 2070-2089.

Yttri, E.A., Wang, C., Liu, Y. & Snyder, L.H. (2014) The parietal reach region is limb specific and not involved in eye-hand coordination. *J. Neurophysiol.*, **111**, 520-532.

## Figure captions

**FIG. 1.** (A) Three-dimensional (3D) reconstructions of the injection area (black outlines) into the ventral lateral intraparietal area (LIPv) or the rostral portion of the medial intraparietal area (MIP), visualized in coronal sections of the brains by Cholera toxin B (CTB) immunolabeling at 2.5 or 3 days after injection of a mixture of rabies and CTB (see A-E). Grey outlines: cortical surface. (Modified with permission from Prevosto *et al.*, *Cereb. Cortex* 2010, 20:214-228 © The Author 2010. Published by Oxford University Press. All rights reserved). The injection area was placed at the midpoint rostrocaudal level of the intraparietal sulcus (IPS) (brain figurines). (B-E) Photomicrographs of adjoining coronal sections at the center of the injection site in MIP (B, C) and LIPv (D, E), immunolabeled for CTB and rabies virus respectively. Note that the injection area is easily identifiable with CTB (B, D) but not with rabies virus (C, E) at 2.5 days, because of strong rabies immunolabeling of short-distance projections neurons in the IPS. In D, shading in the white matter ventral to LIPv is background staining of an area of fibrosis due to multiple recording traces in that region (clearly individualized by cresyl violet counterstaining in E). Similarly, in B and C, zones of fibrosis due to multiple recording traces are seen in the white matter dorsomedial to the MIP injection site. Scale bars in A-E: 2000  $\mu\text{m}$ .

**FIG. 2.** Summary of the pathways of retrograde transneuronal transfer of rabies virus to the vestibular nuclei, medial reticular formation and Scarpa's ganglia after injection of a mixture of rabies virus and Cholera toxin B, CTB into the left medial intraparietal area (MIP) or ventral lateral intraparietal area (LIPv): 1° (light grey), first-order neurons (conventional tracer, CTB) in the ipsilateral thalamus and cortical areas (ipsilateral cortico-cortical inputs, callosal inputs from homotopic IPS areas). 2° (black), second-order neurons labeled



transneuronally (rabies virus) at 2.5 days in the vestibular nuclei and medullary medial reticular formation bilaterally, in the ipsilateral thalamic nuclei and reticular thalamic nucleus, and in the contralateral thalamic nuclei (the latter reflecting projections to homotopic areas in the intraparietal sulcus, IPS, of the right hemisphere). For inputs from the vestibular nuclei and medial reticular formation, line thickness and marker size indicate the strength of the projections. Note the differences in strength and laterality of disynaptic ( $2^\circ$ ) inputs from vestibular nuclei and medial reticular formation to MIP compared with LIPv.  $3^\circ$  (grey), third-order neurons labeled at 3 days bilaterally in Scarpa's ganglia, in the vestibular nuclei, reticular formation and in the thalamus after MIP injection. NB: Third-order inputs to LIPv were not studied (stippled gray lines and open markers in LIPv diagram). Contrary to retrograde transneuronal transfer of rabies virus ( $2^\circ$ ,  $3^\circ$ ), anterograde transneuronal transfer (e.g., to the pontine nuclei) did not occur.

**FIG. 3.** Cross sections and photomicrographs of the ipsilateral and contralateral intraparietal sulcus (IPS) at the caudal end of the injection area, showing the distribution of neurons (first-order) labeled by retrograde transport of Cholera toxin B (CTB) at 2.5 days after injection of a mixture of rabies virus and CTB into the left ventral lateral intraparietal area (LIPv) (A, B) or medial intraparietal area (MIP) (C-F) (see injection site in Fig. 1). Each marker indicates one labeled neuron. (A, B) LIPv: many CTB labeled neurons were seen ipsilaterally (A) in LIPv, in a portion of dorsal LIP (LIPd) and in the ventral intraparietal area (VIP); little labeling was found contralaterally in the homotopic LIPv (B). (C-F) MIP: distribution of labeled neurons in ventral MIP and neighboring dorsal VIP ipsilaterally (C, E), and in the homotopic ventral MIP contralaterally (D, F). Framed areas in (C) and (D), are enlarged in the photomicrographs in (E) and (F), showing examples of CTB labeled neurons in ipsilateral VIP and contralateral MIP, respectively. Scale bars: 2000  $\mu\text{m}$  (A-D), 50  $\mu\text{m}$  in (E) and (F).

**FIG. 4.** Histograms of first-order neurons (Cholera toxin B, CTB) in the ipsilateral thalamus (A) and in homotopic areas of the contralateral intraparietal sulcus (IPS) (B) after injection into the left medial intraparietal area (MIP, at 2.5 days, black, and 3 days, grey, top) or the ventral lateral intraparietal area (LIPv) (2.5 days, black, bottom) (see also Fig. 3). (A) Left thalamus: differences in rostrocaudal distribution of first-order neurons targeting MIP (top) versus LIPv (bottom). Asterisks indicate the most caudal cross section of the thalamus shown in Fig. 5. (B) Callosal projections to MIP and LIPv from homotopic areas of the right IPS and neighboring portions. Note the major difference in cell numbers in the MIP versus LIPv experiments (underlined: rostrocaudal extent of the injection area in the left IPS, see Fig. 1. Asterisks as in A). CTB cell counts are from one series of sections (spacing 400  $\mu$ m). The total number of labeled cells is indicated in each histogram.

**FIG. 5.** Thalamus (coronal sections): Combined visualization of first-order neurons (Cholera toxin B, CTB, white dots), and higher-order thalamic populations (rabies virus: second-order at 2.5 days; third-order at 3 days) after injection of a mixture of rabies virus and CTB into the ventral portion of the lateral intraparietal area (LIPv) or the medial intraparietal area (MIP) of the left hemisphere. Numbers at bottom left corner of each section indicate the distance from the interaural axis, and were computed from sections spacing and thickness and their correspondence with the anteroposterior levels shown in the atlas of Olzewski (1952) with regard to the thalamic nuclei cytoarchitecture and the location of key structures. White dots: first-order neurons (CTB labeling); note the topographical differences of first-order populations targeting LIPv (in central lateral, CL, medial dorsal, MD, lateralis posterior, LP and anterior pulvinar, APul nuclei) versus MIP (more dorsal and lateral, in CL, MD, LP, APul, and also in ventral lateral, pars postrema, VLps, ventral posterior lateral nucleus, pars caudalis, VPLc, and, to a small extent, ventral lateral nucleus, pars caudalis, VLc). Note the

similarity in distribution of first-order thalamic labeling in the two MIP experiments. Dark patches in the photomicrographs: rabies retrograde transneuronal labeling. At 2.5 days rabies immunolabeling is found in the reticular thalamic nucleus (Rt) ipsilaterally (second-order) and other second-order thalamic nuclei bilaterally. The contralateral Rt (third-order) is labeled at 3 days (MIP, right column) and not at 2.5 days, showing that third-order labeling is obtained only at the 3 days time point. Other abbreviations: see Abbreviations list. Scale bars: 2000  $\mu\text{m}$ .

**FIG. 6.** Serial cross sections (400  $\mu\text{m}$  spacing) through the brainstem from caudal (A) to rostral levels (L), showing the distribution of second-order neurons that target disynaptically the medial intraparietal area (MIP), labeled by retrograde transneuronal transfer of rabies virus at 2.5 days. Each dot indicates one labeled neuron. Labeling involves bilaterally the vestibular complex, especially the medial vestibular, magnocellular division (MVmc) and lateral portions of the medial vestibular, parvocellular (MVpc) nuclei. Some labeled cells are also present in descending vestibular (DV), superior vestibular (SV), lateral vestibular (LV) nuclei and vestibular Y group (Y). Bilateral labeling is also found in the medial reticular formation, especially in dorsal paragigantocellular reticular formation (DPGi) and dorsal portions of gigantocellular reticular formation (Gi). A few labeled neurons are also found dorsally in the lateral reticular formation near the rostral MVmc (levels I-J), and other reticular regions. Labeling obtained in prepositus hypoglossi (PH) and dorsal column nuclei (cuneate pars triangularis, CuT, A and external cuneate, ECu, level A) was already described (see Prevosto *et al.*, 2009, 2011). See also the photomicrographs in Fig. 7, and histograms in Fig. 8. Other abbreviations: see Abbreviations list. Scale bar: 2000  $\mu\text{m}$ .

**FIG. 7.** Photomicrographs showing rabies immunolabeled second-order neurons in the vestibular nuclei (VN) and medial reticular formation (dorsal paragigantocellular reticular formation, DPGi, and gigantocellular reticular formation, Gi) that target disynaptically the medial intraparietal area (MIP) (2.5 days). Four different rostrocaudal levels are illustrated. Framed areas in low power views are enlarged. (A) to (D) Rostral medulla (level shown in Fig. 6I): only a few rabies immunolabeled neurons are seen bilaterally in the rostral VN, in the medial vestibular nucleus, magnocellular (MVmc, individual cells are enlarged in the insets in A). Frames in (A) are enlarged in (B), (C) and (D). Note labeled cells in DPGi and Gi (B and C), Asterisks in (A) and (D) point to a dorsal reticular region known to receive a few direct vestibular afferents (see text). (E) and (F) (level shown in Fig. 6G): note at this level many rabies immunolabeled neurons in the VN bilaterally, especially contralaterally, in MVmc and descending vestibular nucleus, DV (frame in E is enlarged in F), and bilateral labeling in Gi (high power views in insets in E). (G) and (H) (level shown in Fig. 6E): in the VN, labeled neurons are most numerous contralaterally in lateral MVmc (frame in G, enlarged in H). Note many labeled neurons bilaterally in Gi and DPGi (individual cells are enlarged in the insets in G). (I) and (J) Caudal medulla (level shown in Fig. 6C): note many labeled cells in contralateral MV (enlarged in inset on the right in I) and bilaterally in Gi and DPGi (high power views in J and in inset on the left in E). Other abbreviations: see Abbreviations list. Scale bars: 1000  $\mu\text{m}$  in (A), (E), (G) and (I), 50  $\mu\text{m}$  in (B), (C), (D), (F), (H), (J) and in all insets in (A), (E), (G) and (I).

**FIG. 8.** Histograms showing the differences in number and distribution of second-order neurons in the vestibular nuclei and medullary reticular formation that target disynaptically the medial intraparietal area (MIP) or the ventral lateral intraparietal area (LIPv) (2.5 days). Left histograms: differences in number and rostrocaudal distribution of second-order neurons

in the medial vestibular (MV) nuclei targeting MIP and LIPv. Sections are numbered (horizontal axis) from the caudal end of the MV. Right histograms: differences in number of second-order neurons in MV, descending vestibular (DV), Y group (Y), superior vestibular (SV), compared with cell counts in the medial reticular formation (dorsal paragigantocellular reticular formation, DPGi and gigantocellular, Gi). Cell counts are from two series of sections (spacing 200  $\mu\text{m}$ ). Black: ipsilateral; gray: contralateral. The total number of labeled cells is indicated on top of each histogram.

**FIG. 9.** Serial cross-sections (400  $\mu\text{m}$  spacing) through the brainstem from caudal (A) to rostral levels (L), showing the distribution of second-order neurons that target disynaptically the ventral lateral intraparietal area (LIPv), labeled by retrograde transneuronal transfer of rabies virus at 2.5 days. Each dot indicates one labeled neuron. A small number of labeled neurons is seen bilaterally in the vestibular complex, especially in the medial vestibular, magnocellular (MVmc) and lateral portions of the medial vestibular, parvocellular (MVpc) nuclei and sparsely in descending vestibular (DV) and superior vestibular (SV) nuclei. Bilateral labeling is also found in the medial reticular formation, in dorsal paragigantocellular reticular formation (DPGi) and dorsal portions of gigantocellular reticular formation (Gi). Some labeled neurons are also found in the lateral reticular formation dorsally, near the rostral MVmc (levels I-J), and ventrally, near the spinal trigeminal nucleus (SpV) (levels C-D). Labeling obtained in SpV, prepositus hypoglossi (PH), and dorsal column nuclei (cuneate triangularis, CuT, A and external cuneate, ECu, A) was already described (see Prevosto *et al.*, 2009, 2011). See also the photomicrographs in Fig. 10, and histograms in Fig. 8. Other abbreviations: see Abbreviations list. Scale bar: 2000  $\mu\text{m}$ .

**FIG. 10.** Photomicrographs showing rabies immunolabeled second-order neurons in the vestibular nuclei (VN) and medial reticular formation (dorsal paragigantocellular reticular formation, DPGi, and gigantocellular reticular formation, Gi) that target disynaptically the ventral lateral intraparietal area (LIPv) (2.5 days). Two different rostrocaudal levels are illustrated. Framed areas in low power views are enlarged. (A) and (B) Rostral medulla (level shown in Fig. 9I): note labeled cells in contralateral DPGi and Gi: frames are enlarged in inset in (A) and in (B). Asterisks point to a dorsal reticular region known to receive a few direct vestibular afferents (see text). (C) and (D) (level shown in Fig. 9G): rabies immunolabeled cells are seen in contralateral Gi and DPGi (insets in C). In the VN, only a few labeled cells are found in the ipsilateral medial vestibular nucleus, magnocellular (MVmc), frame in (C) is enlarged in (D). Other abbreviations: see Abbreviations list. Scale bars: 1000  $\mu\text{m}$  in (A) and (C), 100  $\mu\text{m}$  in (B) and in inset in (A), 50  $\mu\text{m}$  in (D) and in insets in (C).

**FIG. 11.** Photomicrographs showing rabies immunolabeled third-order neurons in the vestibular (Scarpa's) ganglia, vestibular nuclei (VN) and medial reticular formation (dorsal paragigantocellular reticular formation, DPGi, and gigantocellular reticular formation, Gi) that target the medial intraparietal area (MIP), labeled at the trisynaptic time point (3 days). In addition to Scarpa's ganglia, three different brainstem levels are illustrated. Framed areas in low power views are enlarged. (A) and (B) Rostral medulla (level shown in Fig. 12I), showing third-order neuronal labeling in the interstitial nucleus of the vestibular nerve (InVIII<sub>n</sub>) (left framed area in A, enlarged in inset), in portions of medial vestibular, magnocellular (MVmc), descending (DV) and superior vestibular nuclei (SV) nuclei and in the medial reticular formation (DPGi and Gi, frame in A is enlarged in B). (C) Medulla, intermediate level (shown in Fig. 12G); bilateral neuronal labeling in Gi and DPGi and in the

VN, with the greatest concentration in the contralateral MVmc. Insets: labeled neurons in ipsilateral MVmc. (D) Third-order neurons labeled in the contralateral and ipsilateral (inset) Scarpa's ganglia. Initial labeling of ganglion cells does not include axons. (E) to (I) Caudal medulla (level shown in Fig. 12D): bilateral labeling in the VN is still most prominent in the contralateral MVmc (framed area in E is enlarged in F). Some labeled cells are found in DV (inset in D), SV and Y group. At this time point, bilateral labeling in the medial reticular formation ipsilaterally (G) and contralaterally (H and I) includes distal cell processes extending into the medial longitudinal fasciculus (mlf). Other abbreviations: see Abbreviations list. Scale bars: 1000  $\mu\text{m}$  in (A), (C) and (E), 200  $\mu\text{m}$  in (G) and (H), 100  $\mu\text{m}$  in (B), (D), (F) and in insets in (A) and (B), 50 $\mu\text{m}$  in (I) and in insets in (D) and (E).

**FIG. 12.** Serial cross-sections (400  $\mu\text{m}$  spacing) through the brainstem from caudal (A) to rostral levels (L), showing retrograde transneuronal labeling of third-order neurons at 3 days (trisyntaptic time point) after injection of rabies virus into the medial intraparietal area (MIP). Each dot indicates one labeled neuron. A great number of labeled neurons is seen bilaterally in the vestibular complex, in the medial vestibular, magnocellular (MVmc) and parvocellular (MVpc) nuclei, descending (DV), superior (SV) and lateral (LV) vestibular nuclei and Y group. Bilateral labeling is also present in dorsal paragigantocellular reticular formation (DPGi) and throughout the gigantocellular reticular formation (Gi), in the lateral reticular formation near the rostral MVmc (levels I,J), and more sparsely elsewhere in lateral reticular formation, especially near the spinal trigeminal nucleus (SpV). At this time point, dense labeling also appears in portions of the SpV, in the lateral reticular nucleus (LRN) (levels A-C), mainly contralaterally, and in the interstitial nucleus of the vestibular nerve (InVIIIIn) bilaterally (levels I,K) (see also Fig. 11A). Labeling obtained in prepositus hypoglossi (PH), and dorsal column nuclei (cuneate triangularis, CuT, A and external cuneate, ECu, A) was

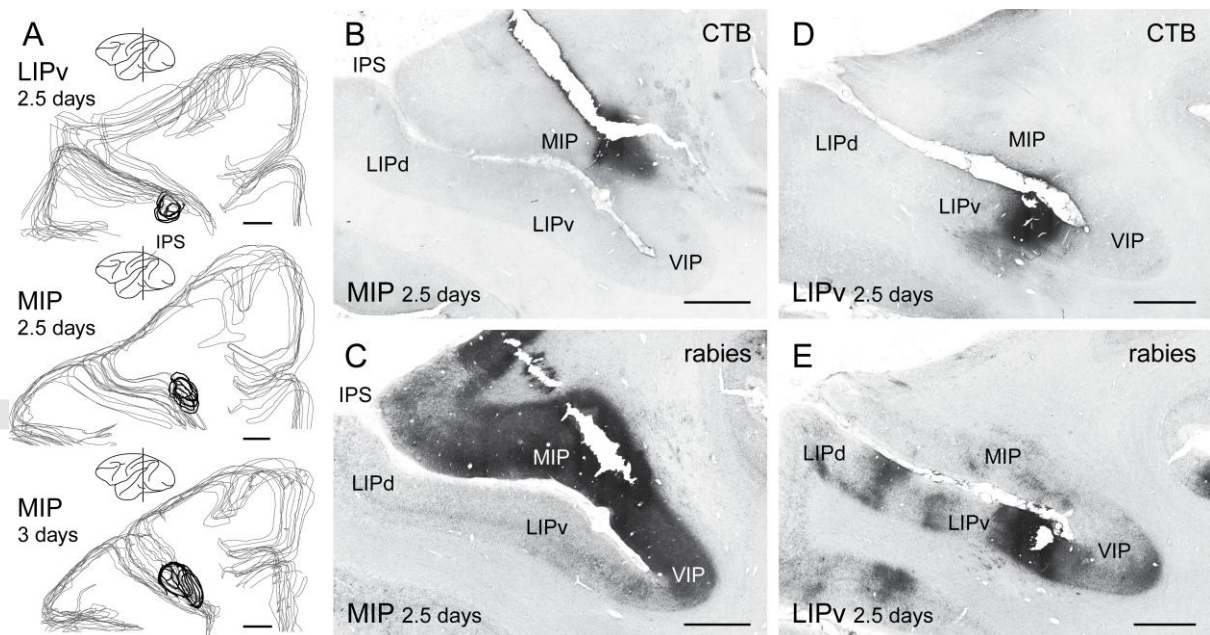
already described (see Prevosto *et al.*, 2009, 2011). See also the photomicrographs in Fig. 11.

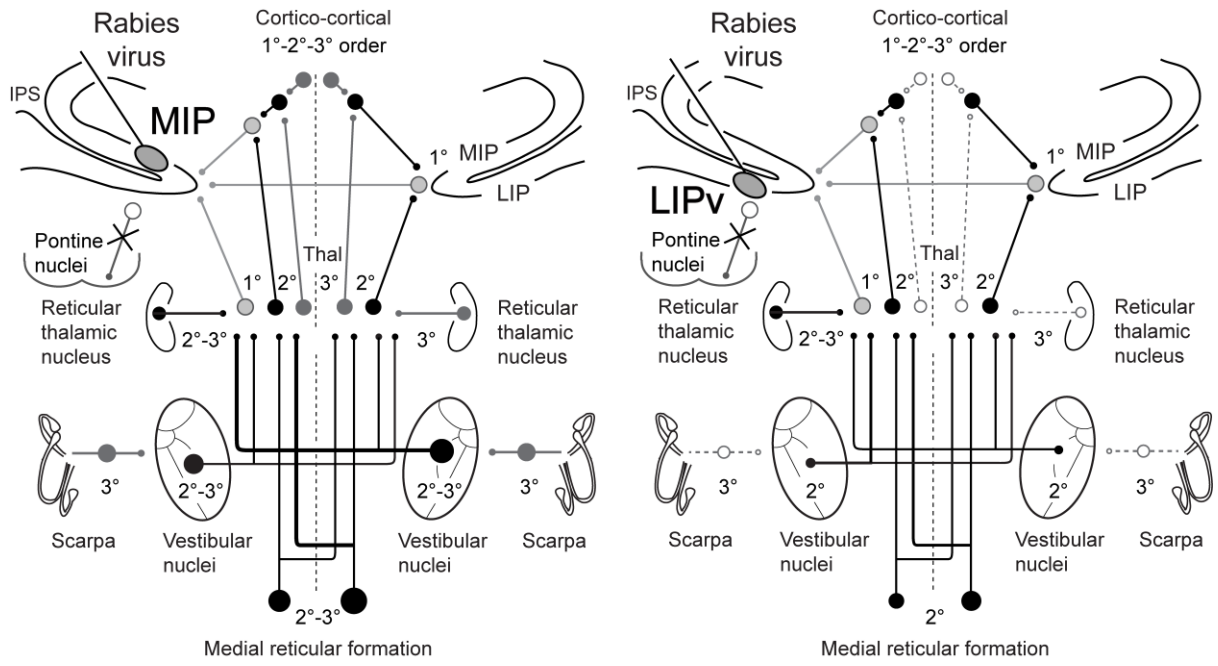
Other abbreviations: see Abbreviations list. Scale bar: 2000  $\mu\text{m}$ .

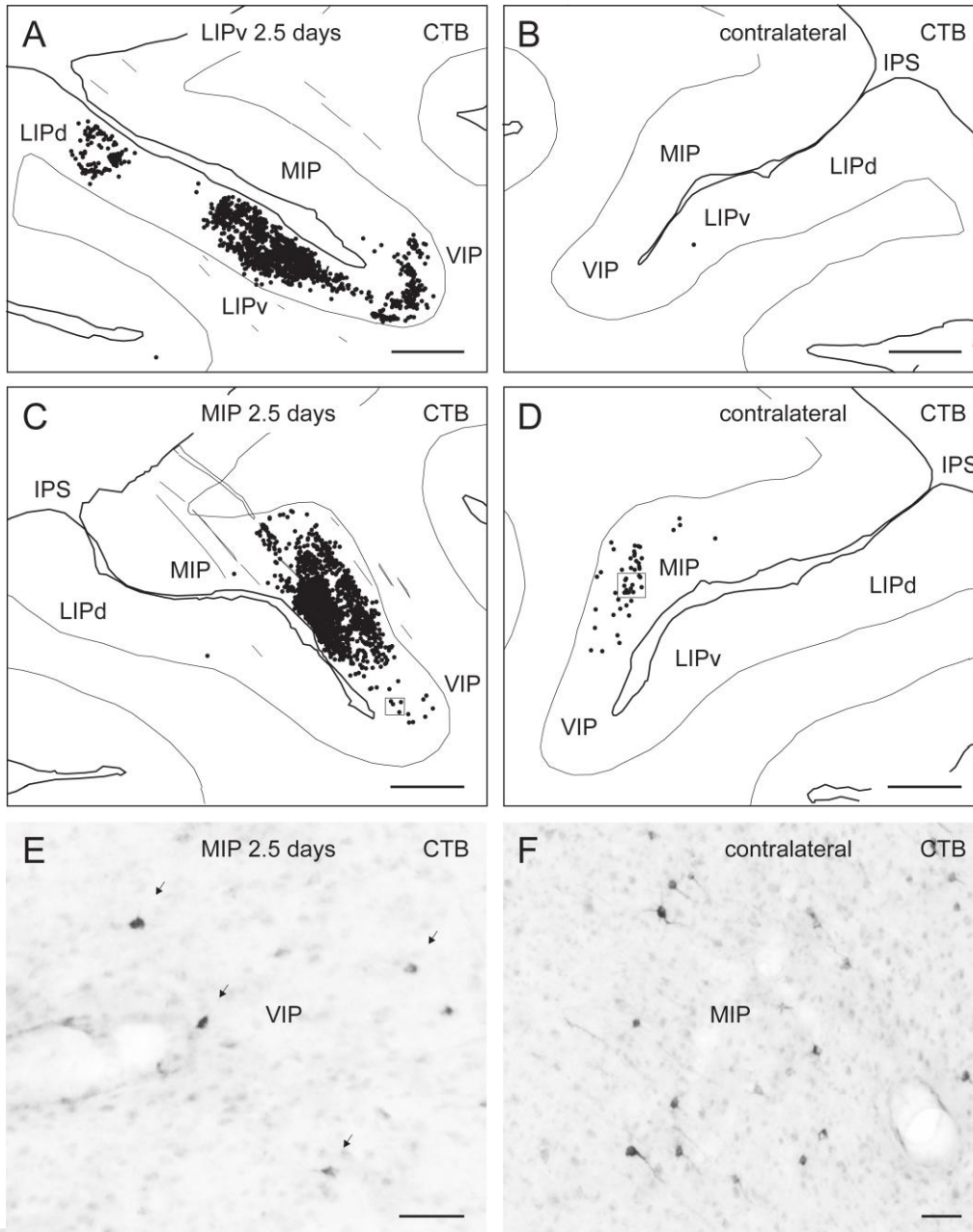
**FIG. 13.** Simplified diagram summarizing ascending polysynaptic pathways to the rostral medial intraparietal area (MIP) (A) or ventral lateral intraparietal area (LIPv) (B) (see text and Prevosto *et al.*, 2009, 2010, 2011). Labeled pathways are shown by black markers, solid lines and large arrows (markers size indicates projection strength). For bilateral pathways only the dominant side is shown. (1°): First-order; (2°) disynaptic pathways; (3°) trisynaptic (in MIP). (A) Inputs to rostral MIP: (a) eye velocity and position signals (prepositus hypoglossi, PH, vertical arrow: caudo-rostral velocity-to-position transformation; Prevosto *et al.*, 2009); (b) arm and neck proprioceptive inputs from the dorsal column nuclei, DCN (2°) (cuneate pars triangularis, CuT, and external cuneate, ECu, Prevosto *et al.*, 2011); (c) efference copy pathways from arm- and head movement-related reticulospinal domains (medial reticular formation, MRF) (2°); (d) vestibular inputs from the vestibular nuclei (VN) (2°) and Scarpa's ganglia (3°) (present study); (e) major cerebellar output channels from dentate (D) and interpositus posterior (IP, arm- and eye movements-related domains, in dark and light grey respectively) (2°) and related cerebellar cortical modules (3°) (dark grey: paramedian lobule, PML/Crus II 50.6%, Simplex/Anterior lobe, AL 26.1%; light grey: dorsal paraflocculus, DPF1 10.6%); note only minor inputs from rostral fastigial (F) and cerebellar vermis, 2.6% (see Prevosto *et al.*, 2010). Rostral MIP and the labeled PH, DCN, VN, MRF and cerebellar domains form a tightly interconnected circuit for multisensory guidance and online control of arm movements and eye-hand coordination coupling (and internal models implying the posterior parietal cortex and cerebellum). Known main interconnections and pathways (unlabeled) are indicated by open markers, stippled lines and small arrows: proprioceptive afferents to DCN, VN, MRF and cerebellum; inputs to the labeled cerebellar

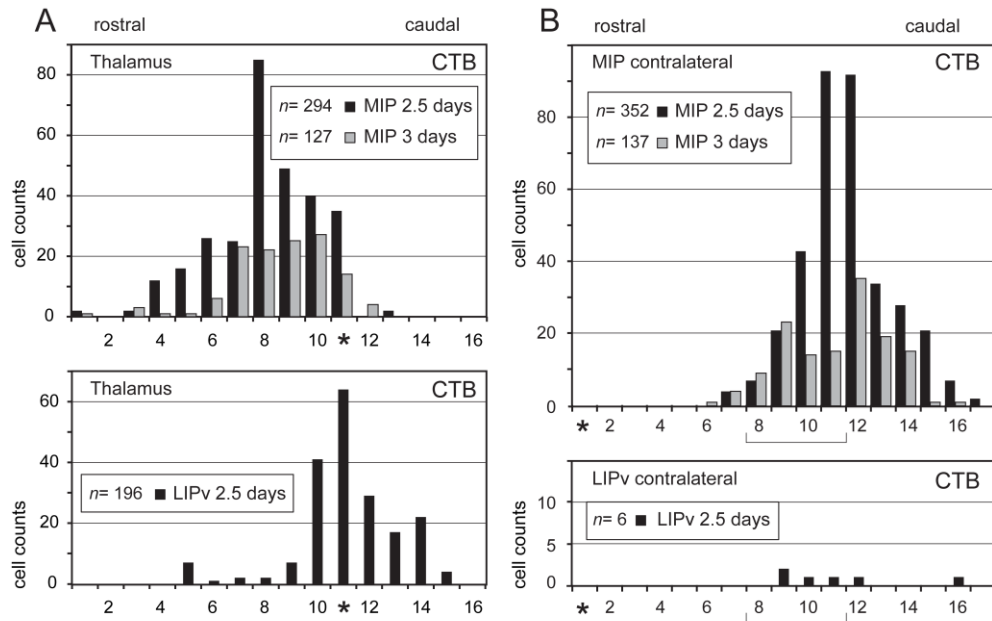


domains from PH, DCN, VN, MRF; (crossed) cerebellar output pathways to VN, MRF and DCN (ECu); VN-MRF interconnections; vestibulo- and reticulospinal pathways; MIP projections to DCN (see text and Prevosto *et al.*, 2009, 2010, 2011). (B) Disynaptic pathways to LIPv carry eye and head movement signals: (a) eye position and velocity inputs (PH); (b) neck proprioceptive (DCN); (c) efference copy signals from the MRF head movement region, and (d) minor vestibular inputs (VN) (neural substrates of eye and head gain fields); (e) cerebellar output channels from the saccade-related caudal ventrolateral IP and caudal dentate (cD) (and not from F) (see text and Prevosto *et al.*, 2009, 2010, 2011). Stippled pathways as in (A). Other abbreviations: CCN, central cervical nucleus; DRG, dorsal root ganglia; IA, Interpositus anterior; IPS, intraparietal sulcus.









LIPv (2.5 d.)  
rabies + CTB (dots)

MIP (2.5 d.)  
rabies + CTB (dots)

MIP (3 d.)  
rabies + CTB (dots)

